Bilateral French-Italy Workshop

Open issues and emerging approaches in geo-environmental mechanics

Organized by

GDRI GeoMech & MEMOCS

Roma, Italy, 2-4 May 2017

Book of extended abstracts

Edited by Pierre-Yves Hicher and Pearl-Angelika Lee

Mechanisms of instability in granular slopes

P.Y. Hicher* and W. Hu**

*Ecole Centrale de Nantes, UMR CNRS GeM
**State Key laboratory of Geohazards Prevention and Geohazards Environmental Protection
Chengdu University of Technology
pierre-yves.hicher@ec-nantes.fr

The 2008 Wenchuan Earthquake in the Sichuan Province, China, generated many landslides which produced a huge amount of loose deposits (Fig.1a). These loose deposits have caused a dramatic increase in debris-flow occurrence in subsequent years. The Wenjia gully debris flow located in the Qingping section of the Mianyuan River was the largest among these debris flows. The loose source material of this debris flow was deposited by a rock avalanche due to the Wenchuan earthquake. The high energy of the rock avalanche was able to entrain the shallow, loose, soil material along its flow path; therefore, the deposited material has a volume of $>7.0\times10^7$ m^3. On the 13th of August 2010, heavy rain generated intensive runoff that produced the debris flow which provoked heavy damages to buildings and infrastructures (Fig. 1b).
Flume tests were performed in order to simulate the whole initiation process and a special attention was given to study the influence of the fine particle content.

Figure 1a. Loose material deposit in Wenjia Gully

Figure 1b. Debris flow in Wenjia Gully

The experimental device consisted of a heavily equipped flume (Fig. 2) 3.5 m in length and 1 m in width (Hu *et al*., 2015, 2016). The side-walls of the flume were made of transparent plexi-glass plates. The bottom was made by gluing calcareous grains on a rubber sheet in order to reproduce an impervious frictional contact. Pore pressure sensors were installed inside the soil layer at different depths and also at the bottom of the flume. The horizontal slope surface movement was monitored by a laser displacement sensor. The internal movement of the slope was measured by an inside movement monitoring system.
The influence of the nature of the soil constituting the slope was analysed by preparing samples with a fines content varying from 0 to 16%. The samples were progressively wetted by a uniform inflow along the rear of the flume. The influence of the fines content was demonstrated by the change in the sliding mechanism that occurred during the tests. For low

fines contents, a circular zone of localised failure was observed, whereas for higher fines contents, the fluidisation of the entire slope was obtained (Hu *et al*, 2017).

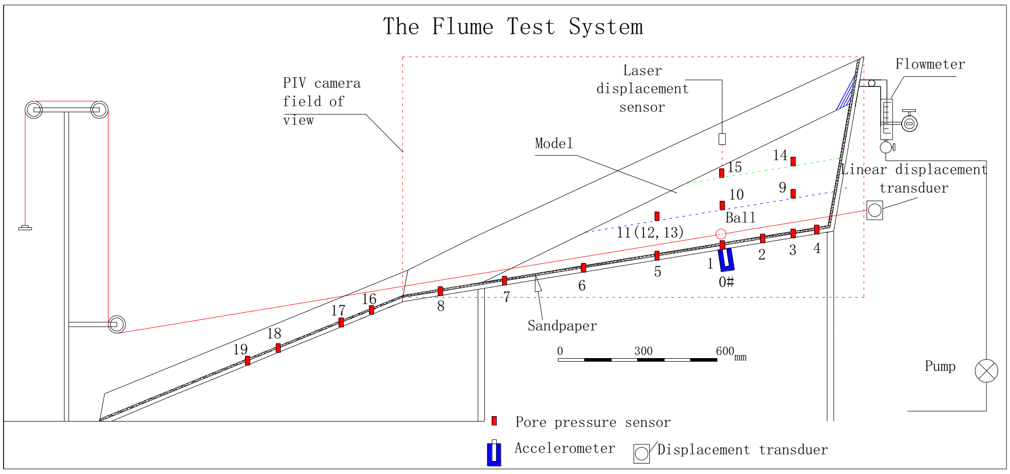

Figure 2. The flume test system

A special attention has been given to the example of the slope failure corresponding to the fluidisation mechanism. Due to water infiltration, the soil at the bottom of the slope became gradually saturated while the pore pressure began to increase. At the same time, due to seepage forces, the bottom material started to erode. Part of the fine particles progressively washed away and the soil structure started to lose its stability. This erosion process could be witnessed in the turbidity of the effluent leaving the flume at the bottom of the slope. Under the double influence of the pore pressure increase and the departure of a part of the fine particles by internal erosion resulting in a looser structure with many macro-voids, a rearrangement of the internal soil structure took place. These macro-voids produced local collapses, inducing a settlement of the soil mass which was measured through the surface movement monitored by the laser displacement sensor. As a consequence, the pore pressure increased at much higher speed. The air bubbles contained in the soil became compressed by the increase of the water pressure and, progressively, the soil reached an almost saturated state which enhanced the pore pressure rise. At that point, the slope began moving rapidly. The diffusion of the pore water could not over-compensate for the growth of its pressure which induced the instability of the soil, finally resulting in a large movement. The response of the soil suddenly evolved from a quasi-static regime toward a dynamic one. The onset of instability was indicated by the development of an autogenous seismicity measured by the accelerometer placed at the bottom of the flume (Hu *et al*, 2017).
It appeared, therefore, that the failure mechanism was controlled by the progressive erosion of the fine particles and that this specific aspect of the slope instability should be better analysed. Triaxial tests were performed on samples with different fines contents, which demonstrated the influence of the fines content on the size of the instability domain.
A numerical approach has been developed in order to deepen our understanding of the sliding mechanism in presence of internal erosion. The micromechanical stress-strain model of Chang and Hicher (2005) has been adapted in order to reproduce the behaviour of sand-silt mixtures (Yin *et al*., 2014). The model takes into account the influence of the fines content on soil dilatancy and strength by formulating the evolution of the critical state line of sand-silt mixtures based on experimental results. Numerical simulations of laboratory tests results showed that the model is able to reproduce the influence of the fines content on the overall

behaviour of sand-silt mixtures, as well as the impact of a decrease of the amount of fines on the mechanical behaviour of eroded silty sand.

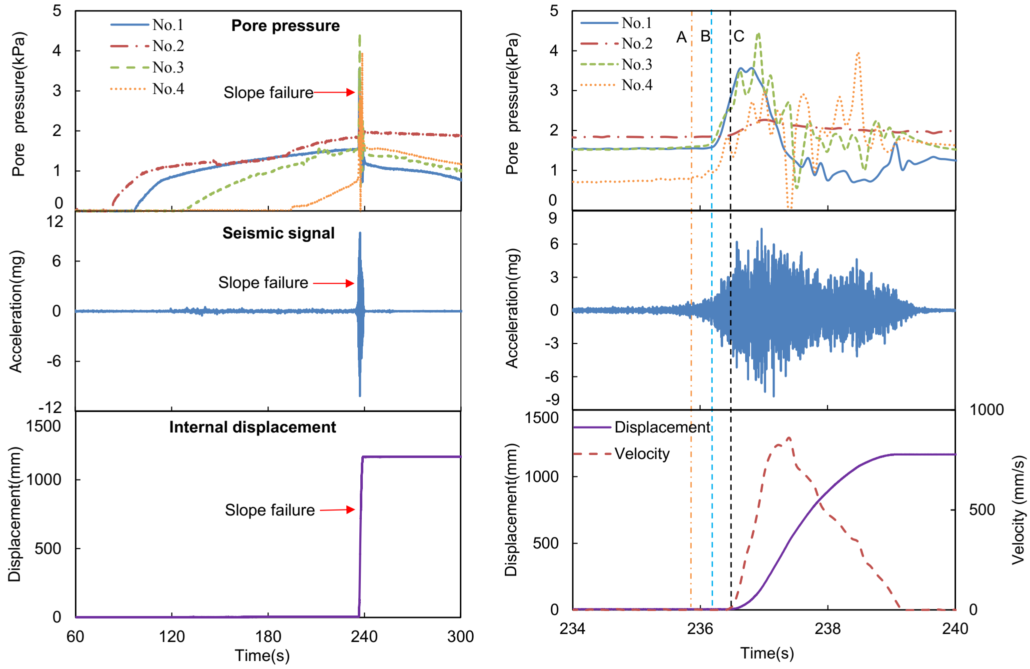

Figure 3. Recording of pore pressure, displacement and vibration during flume test; a, monitoring from 60 seconds to 300 seconds; b, monitoring from 234 seconds to 240 seconds, corresponding to the collapse of the slope.

References

Chang, C. & , Hicher, P-Y. (2005) An elastoplastic Model for Granular Materials with Microstructural Consideration, *International Journal of Solids and Structures*, Vol. 42(14), pp. 4258-4277.

Yin, Z-Y., Zhao, J., Hicher, P-Y. (2014) A micromechanics-based model for sand-silt mixtures, *International Journal of Solids and Structures*, Vol. 51(6), pp 1350-1353.

Hu, W., Xu, Q., Wang, G. H., van Asch, T. W. J & Hicher, P-Y. (2015) Sensitivity of the initiation of debris flow to initial soil moisture, *Landslides*, Vol. 12(6), pp 1139–1145

Hu, W., Dong, X.J., Xu, Q., Wang, G.H., van Asch, T.W.J., Hicher, P-Y., (2016) Initiation processes for run-off generated debris flows in the Wenchuan earthquake area of China, *Geomorphology*, Vol. 253, pp 468-477.

Hu, W. Hicher, P.-Y., Scaringi, G., Xu, Q., van Asch, T. (2017) Seismic precursor to instability induced by internal erosion in loose granular slopes. *Geotechnique* (in press).

Hu, W., Scaringi, G., Xu, Q., Pei, Z., van Asch, T., Hicher, P.-Y. Sensitivity of the initiation and runout of flowslides in loose granular deposits to the content of small particles: An insight from flume tests. *Engineering Geology* http://dx.doi.org/10.1016/j.enggeo.2017.10.001

From microscale to boundary value problems: using a micromechanically-based model

Hao Xiong* & Francois Nicot* & Zhenyu Yin**

**Université Grenoble Alpes, IRSTEA, Geomechanics Group, ETNA, Grenoble, France*

***LUNAM University, Ecole Centrale de Nantes, UMR CNRS GeM, Nantes, France*

hao.xiong@irstea.fr

Granular materials represent significant issues for geotechnical engineering, generating considerable research to observe, investigate and understand their complex behavior when subjected to loading paths. One of the phenomena observed refers to the instability occurrence, related to two kinds of failure modes: localized and diffuse (Daouadji *et al.*, 2011). The associated bifurcation at the material point level is conventionally associated with the stress peak of a strain softening material or at the plastic threshold. The problem underlies a material instability phenomenon that originates at the small-scale due to the micro-structural features of the granular material. Therefore, developing a micromechanically-based constitutive model of granular material is desired.

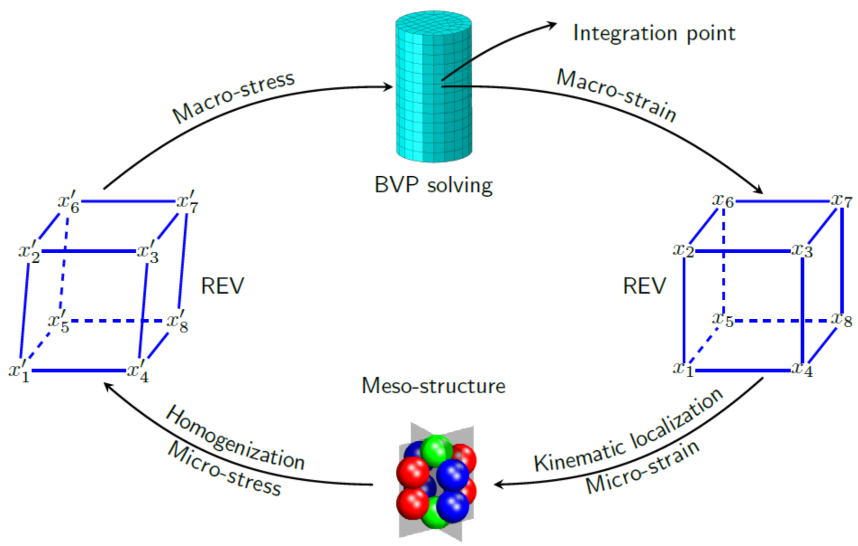

Figure 1. The schematic diagram of multi-scale approach.

A 3D multi-scale approach is presented to investigate the mechanical behaviour of a macroscopic specimen consisting of a granular assembly, as a boundary value problem. The core of this approach is a multi-scale coupling (Figure 1), wherein the finite element method is used to solve a boundary value problem and a micromechanically-based model (Xiong and Nicot, 2017) is employed to build the micro constitutive relationship used at a representative volume element scale. This approach provides a convenient way to link the macroscopic observations with intrinsic microscopic mechanisms. The plane-strain biaxial loading condition (Figure 2) is selected to simulate the strain localization. A series of tests are performed, wherein distinct failure patterns are observed and analysed. A system of shear band naturally appears in a homogeneous setting specimen, with the result that the specimen bifurcate from a homogeneous condition to a non-homogeneous condition (Figure 3). By defining the shear band area, microstructural mechanisms are separately investigated inside and outside the shear band. Moreover, a second-order work directional analysis is performed by applying strain probes at different stress-strain states along drained biaxial loading paths. The normalized second order work introduced as an indicator of unstable trend of the system is analysed not only at the macroscale but also at the microscale.

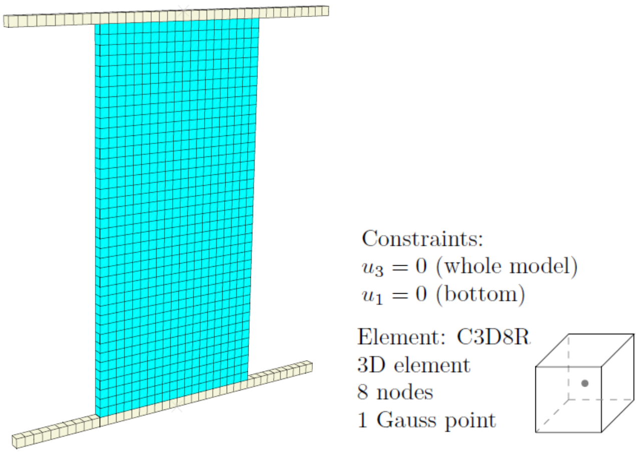

Figure 2. Model constraints and element type.

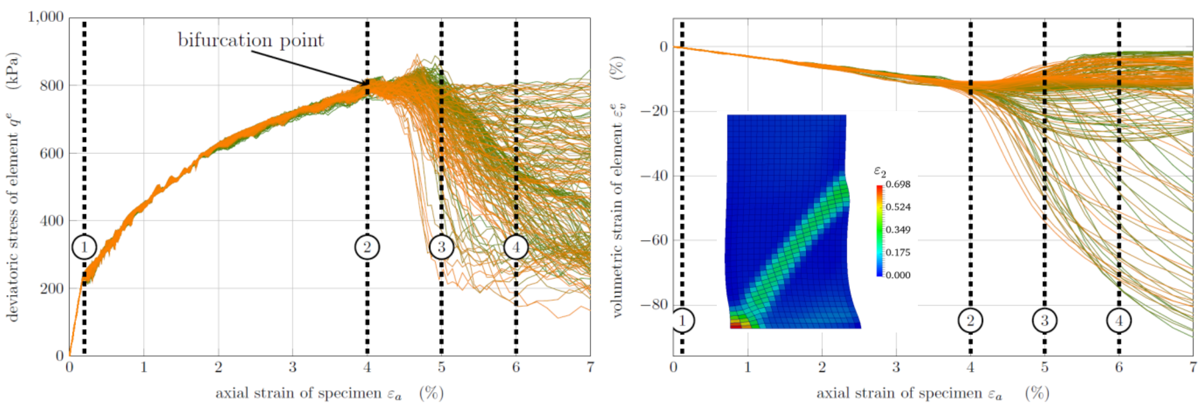

Figure 3. Mechanical and volumetric responses of all elements in the finite element mesh.

References

Xiong, H., Nicot, F., and Yin, Z. Y., 2017. A three-dimensional micromechanically based model. *International Journal for Numerical and Analytical Methods in Geomechanics.*

Daouadji, A., Darve, F., Al Gali, H., Hicher, P. Y., Laouafa, F., Lignon, S., ... & Sibille, L., 2011. Diffuse failure in geomaterials: Experiments, theory and modelling. *International Journal for Numerical and Analytical Methods in Geomechanics*, 35(16), 1731-1773.

Modelling the influence of microstructure on failure in granular soils using a multiscale approach

G. Veylon* & F. Nicot**

**Irstea, Civil Engineering Group, Aix-en-Provence, France*
*** Irstea, Geomechanics Group, Grenoble, France*
guillaume.veylon@irstea.fr

Granular materials generally exhibit a broad spectrum of mechanical properties. Developing constitutive models to integrate these properties in the context of simulations at the structural scale remains a scientific challenge. In this respect, multi-scale approaches offer very promising perspectives, as they allow the emergence of macroscopic properties from micromechanical models calibrated at a microscopic scale.

Among the multiscale models, the H-Model (Nicot & Darve, 2011) marks a major step forward in taking into account the effects of the microstructure on the behaviour of granular materials. The structure of the granular material is described by an assembly of hexagons, the orientation of which is distributed in the physical space. From homogenization operations, incremental stress and strain are inter-related at the assembly scale, giving rise to a constitutive model that has the ability to reproduce the essential mechanical properties of granular materials.

The H-Model was implemented into a finite difference software. Simulations of non-homogeneous biaxial tests were carried out in order to explore the model's capacities to reproduce the different failure modes observed in the laboratory. The use of the H-Model to simulate drained and undrained biaxial tests highlights the influence which the microstructure has on the mechanical response of granular materials. Finally, the H-Model is used at the engineering scale (boundary value problems) to model the loading of a shallow foundation.

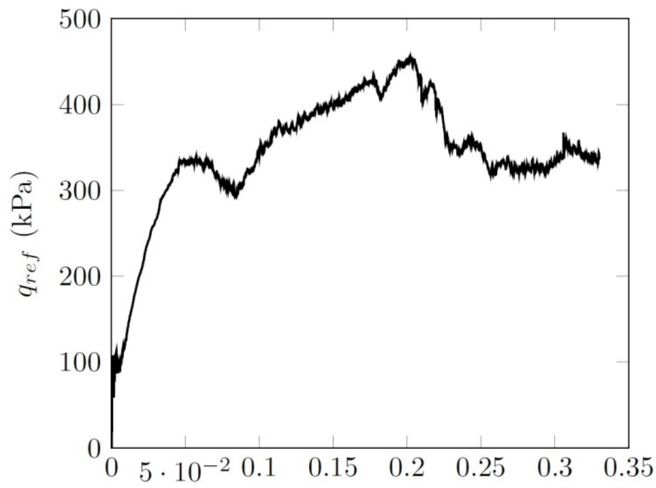

(a)

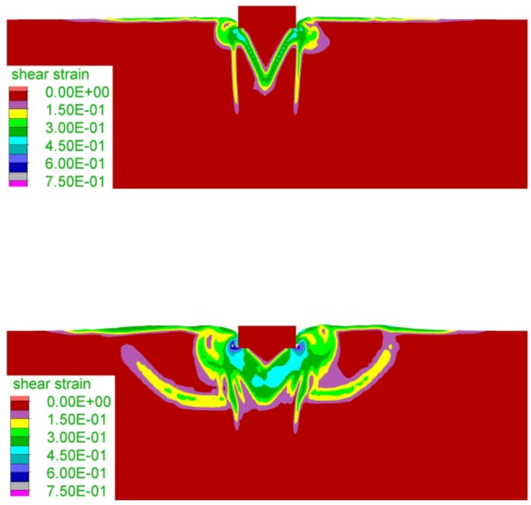

(b)

Figure 1. Modelling of a one meter width shallow foundation using the H-Model: (a) mean vertical stress q_{ref} as a function of the settlement (m) ; (b) shear strain field within the foundation for settlement equal to 15 cm (above) and 30 cm (bellow)

References

Nicot, F. (2003): Constitutive modelling of a snowcover with a change in scale. *European Journal of Mechanics (A /Solids)*, 22-3, 325–340.

Nicot, F., and Darve, F. (2005): A multiscale approach to granular materials. *Mechanics of Materials*, 37 (9), 980–1006.

Nicot, F., Darve, F. (2011). The H-microdirectional model: Accounting for a mesoscopic scale. *Mechanics of Materials, 43*, 918–929.

Veylon, G. (2017). Modélisation numérique du mécanisme de liquéfaction des sols – Application aux ouvrages hydrauliques. *PhD thesis, Université Grenoble Alpes*, 200 p.

Zhu, H., Veylon, G., Nicot, F., Davre, F. (2016). On the mechanics of meso-scale structures in two-dimensional granular materials. *European Journal of Environmental and Civil Engineering*, 21(7-8), 912–935.

Applying thermodynamic principles to multiscale modelling of unsaturated granular soils

Chaofa Zhao, Younes Salami, Zhen-Yu Yin & Pierre-Yves Hicher

Ecole Centrale de Nantes, UMR CNRS GeM. 1, rue de la Noë - B.P. 92101, 44321 Nantes Cedex 3, France.
Emails: chaofa.zhao/younes.salami/zhenyu.yin/pierre-yves.hicher@ec-nantes.fr

Unsaturated granular soils are three-phase granular materials composed of soil particles, water and air. Consequently, the macroscopic behaviour of unsaturated granular soils is highly dependent on the characteristics of the components and their interactions. Generally, solid particles and fluid are assumed to be incompressible, whereas air is compressible. Three interaction pairs, *i.e.* solid and fluid, solid and air, fluid and air have been considered. The effect of these interactions is typically considered in the form of a capillary force exerted by the water menisci between particles. The magnitude of the capillary force, which relates to degree of saturation, can cause significant changes in volume, shear strength and hydraulic properties of granular soils (Sheng, 2011).

The constitutive behaviour of unsaturated soils has been extensively studied in the last three decades (Alonso *et al*., 1990; Wheeler & Sivakumar, 1995; Cui & Delage, 1996; Sheng *et al*., 2004; Sheng, 2011). The early developments tended to adopt net stress and suction as independent stress variables and to extend the available elastoplastic models to saturated soils by introducing suction-dependent compressibility and yield surface (*e.g*., Alonso *et al*., 1990; Cui & Delage, 1996; Sheng *et al*., 2004). The first example is the Barcelona Basic Model (BBM), suggested by Alonso *et al*. (1990), in which a suction-dependent loading collapse curve (LCC) was introduced based on the modified Cam-clay model. Alternatively, many attempts have been made to define an effective stress in order to represent the deformation of the soil skeleton for unsaturated soils (Bishop & Blight, 1963; Zhao *et al*., 2010). By using the effective stress concept, the hydraulic hysteresis phenomenon and the transitional behaviour from the unsaturated to the saturated state can be captured effectively.

From a physical point of view, the formation of water menisci located between neighbouring grains produces capillary forces on the grains. Based on these observations, the CH micromechanical model (Chang & Hicher, 2005) for saturated granular soils was extended to study the hydro-mechanical behaviour of unsaturated granular materials (Hicher & Chang, 2007). In this model, the capillary forces between inter-particle contacts are assumed to be dependent on the degree of saturation and integrated with the same homogenization method as for the mechanical forces. A tensor type capillary stress has thus been defined and proven to be an efficient alternative to suction (Hicher & Chang, 2007; Scholtès *et al*., 2009).

Since the thermodynamic approach involving internal variables forms a coherent framework within which constitutive relations can be developed without the need for *ad hoc* assumptions and procedures, various studies have produced constitutive models consistent with it (Li, 2007; Coussy *et al*., 2010; Dangla & Pereira, 2014). By analysing the work input on an unsaturated representative volume element, the effective stress could be derived and conjugated to the deformation of the solid skeleton (Houlsby, 1997; Zhao *et al*., 2010; Li *et al*., 2017), with the assumption that the surface energy change is equal to the energy necessary for moving the air-water interface during the invasion process with the matric suction becoming a function of the water saturation (Coussy *et al*., 2010).

This study aims to develop the thermodynamic approach for multiscale modelling of the unsaturated granular soils by considering the energy to dissipate through friction at the inter-particle contacts during loading. The energy conservation at the micro and macro scales is firstly presented, after which the separation of the energy into a mechanical and a hydraulic part is discussed. The thermodynamically consistent CH micromechanical model is adopted for the mechanical deformation of the solid skeleton, while a particle size dependent potential function is responsible for the hydraulic part. The presented constitutive model has been published in the Proceedings of 6th Biot Conference (Zhao *et al*., 2017).

References

Alonso, E. E., Gens, A., and Josa, A., 1990. Constitutive model for partially saturated soils. *Géotechnique*, 40(3), pp.405-430.

Bishop, A. W. and Blight, G. E., 1963. Some aspects of effective stress in saturated and partly saturated soils. *Géotechnique*, 13(3), pp.177-197.

Chang, C. S. and Hicher, P. Y., 2005. An Elasto-plastic Model for Granular Materials with Microstructural Consideration. *International Journal of Solids and Structures*, 42(14), pp.4258 -4277.

Coussy, O., Pereira, J. M., and Vaunat, J., 2010. Revisiting the thermodynamics of hardening plasticity for unsaturated soils. *Computers and Geotechnics*, 37(1), pp.207-215.

Cui, Y. J. and Delage, P., 1996. Yielding and plastic behaviour of an unsaturated compacted silt. *Géotechnique*, 46(2), pp.291-311.

Dangla, P. and Pereira, J. M., 2014. A thermodynamic approach to effective stresses in unsaturated soils incorporating the concept of partial pore deformations. *Vadose Zone Journal*, *13*(5), pp.1-11.

Hicher, P. Y. and Chang, C.S., 2007. A microstructural elastoplastic model for unsaturated granular materials. *International Journal of Solids and Structures*, 44(7), pp.2304-2323.

Houlsby, G. T., 1997. The work input to an unsaturated granular material. *Géotechnique*, 47(1), pp.193-196.

Li, J., Yin, Z. Y., Cui, Y. J. and Hicher, P. Y., 2017. Work input analysis for soils with double porosity and application to the hydro-mechanical modeling of unsaturated expansive clays. *Canadian Geotechnical Journal*, 54(2), pp.173-187.

Li, X. S., 2007. Thermodynamics-based constitutive framework for unsaturated soils. 1: Theory. *Géotechnique*, 57(5), pp.411-422.

Scholtès, L., Hicher, P. Y., Nicot, F., Chareyre, B. and Darve, F., 2009. On the capillary stress tensor in the pendular regime of wet granular materials. *International Journal for Numerical and Analytical Methods* in Geomechanics, 33(10), pp.1289-1313.

Sheng, D., 2011. Review of fundamental principles in modelling unsaturated soil behaviour. *Computers and Geotechnics*, 38(6), pp.757-776.

Sheng, D., Sloan, S. W. and Gens, A., 2004. A constitutive model for unsaturated soils: thermomechanical and computational aspects. *Computational Mechanics*, 33(6), pp.453-465.

Wheeler, S. J. and Sivakumar, V., 1995. An elasto-plastic critical state framework for unsaturated soil. *Géotechnique*, 45(1), pp.35-53.

Zhao, C., Salami, Y., Yin, Z.Y. and Hicher, P.Y., 2017. A micromechanical model for unsaturated soils based on thermodynamics. *In Poromechanics VI*, pp.594-601.

Zhao, C. G., Liu, Y. and Gao, F. P., 2010. Work and energy equations and the principle of generalized effective stress for unsaturated soils. *International Journal for Numerical and* Analytical Methods in Geomechanics, 34(9), pp.920-936.

A microstructured continuum for dissipation phenomena in concrete using a multi-scale model with rate-dependent internal friction

I. Giorgio* & D. Scerrato*

**International Research Center for the Mathematics and Mechanics of Complex Systems, M&MoCS, University of L'Aquila, L'Aquila, Italy*
Ivan.giorgio@uniroma1.it

A micromorphic, non-linear 3D model aiming to describe internal friction phenomena in concrete is proposed. A reduced two-degrees-of-freedom model is employed to explain dissipative loops which have been observed in some concrete specimens tested under cyclic uniaxial compression loading with different frequencies and various amplitudes but never inducing large strains. As viscoelastic models, linear or non-linear, do **not** seem suitable to describe either qualitatively or quantitatively the measured dissipation loops, we propose to introduce a multi-scale micromechanism of Coulomb-type internal dissipation associated to the relative motion of the faces of the micro-cracks present in the material and to the asperities inside the micro-cracks. To obtain a proper kinematical description aiming to describe internal friction phenomena, we choose the common variable $\boldsymbol{u}$ as a displacement field (and the related strain deformation along the longitudinal axis of a cylinder, ε), the meso-structural variable φ as a scalar field, which is interpreted as the relative displacement between two opposite faces of micro-cracks, and the micro-structural variable z as a scalar field which describe the collective asperity deformation (figure 1).

In the case of a compressive test, the principle of virtual work for any arbitrary virtual strain $\delta\varepsilon$ and virtual micro-sliding $\delta\varphi$ provides, assuming an evolution rule for the variable z:

$$\begin{cases} M_\varepsilon \ddot{\varepsilon} + K_\varepsilon \varepsilon + \alpha\varphi = f^{ext}(t) \\ m_\varphi \ddot{\varphi} + (k_1\varphi + k_2\varphi^2 + k_3\varphi^3) + \alpha\varepsilon + (\gamma_0 z + \gamma_1 \dot{z} + \gamma_2 \dot{\varphi}) = 0 \\ \dot{z} = \dot{\varphi}\left|1 - \dfrac{z}{\delta(\varepsilon,\dot{\varphi})} sgn(\dot{\varphi})\right|^\beta sgn\left(1 - \dfrac{z}{\delta(\varepsilon,\dot{\varphi})} sgn(\dot{\varphi})\right) \end{cases}$$

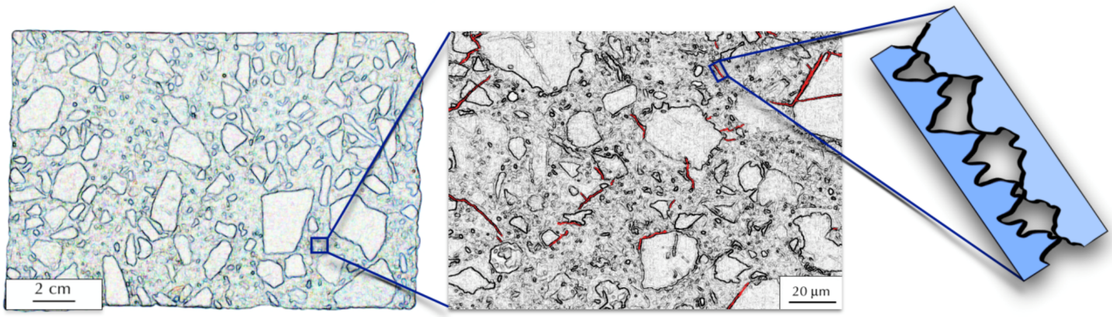

Figure 1. Three scale representation.

Figure 2 shows the dissipative loops in a stress-strain plane obtained varying frequency with numerical simulations. In this range of frequencies, we observe that the dissipation energy, i.e. the area of the loops, decreases with increase of frequency. That particular behavior – indeed, is opposite to the behavior expected for a viscous dissipation– matches with measured cycles showing a sort of Stribeck's effect.

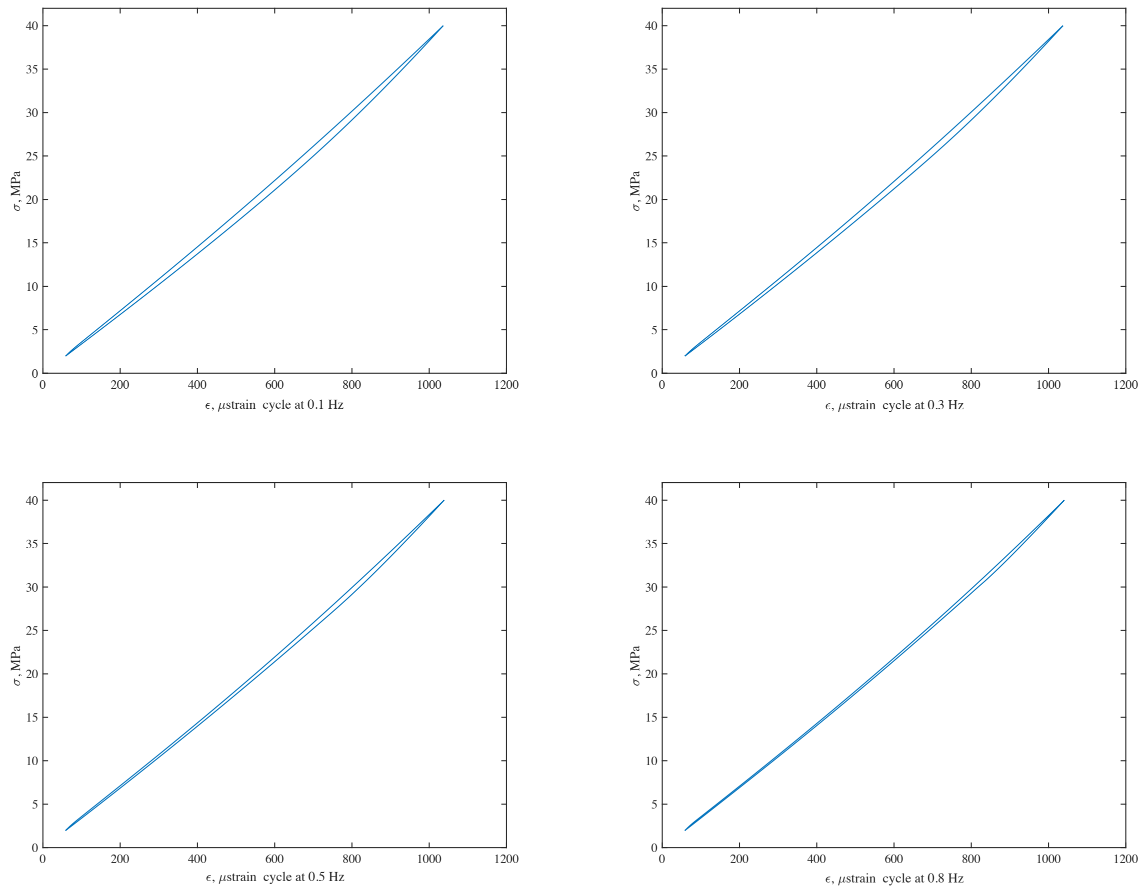

Figure 2. Simulated dissipative loops for a concrete mixture and frequencies 0.1 Hz, 0.3 Hz, 0.5 Hz and 0.8 Hz.

References

Scerrato, D., Giorgio, I., Madeo, A., Limam, A. and Darve, F., 2014. A simple non-linear model for internal friction in modified concrete. *International Journal of Engineering Science*, 80, pp. 136–152.

Giorgio, I. and Scerrato, D., 2017. Multi-scale concrete model with rate dependent internal friction. *European Journal of Environmental and Civil Engineering*, 21(7–8), pp. 821–839.

Sustainability of the Meso-structure in Granular Materials during Shear Band Forming

J. Liu[*,], F. Nicot[**] & W. Zhou[*]**

**State Key Laboratory of Water Resources and Hydropower Engineering Science, Wuhan University, Wuhan 430072, China*
***Université Grenoble-Alpes, IRSTEA, ETNA Geomechanics Group, Grenoble 38402, France*
Email: liujy@whu.edu.cn ; jiaying.liu@irstea.fr (Jiaying Liu)

For frictional granular geomaterials, the shear band and the strain localization are essential problems for constitutive modelling (Nicot and Darve, 2011). When shear bands form, spatial heterogeneity develops and non-affined deformation takes place. Perspectives at the meso-scale (Zhu *et al.*, 2016a,b; Tordesillas *et al.*, 2008; Nguyen *et al.*, 2012) are expected to reveal the underlying mechanism of strain localization. The sustainability of the granular system at a material point has primarily been related to the stress and strain state. The notion of loss of sustainability has been developed in relation to the increase of the kinetic energy and the zero or negative second-order work W_2 (Nicot and Darve, 2007; Nicot *et al.*,2007). At the mesoscopic scale, sustainability could be regarded as a topological and geometrical change for a single element, e.g., loops and force chains. As deviatoric loads are applied, force chains can be buckled and the loops may disappear or they may transform to different sizes.

This study emphasizes the evolution and exchanges of meso-structures during the shear band formation. A 2D biaxial DEM simulation has been conducted for a dense specimen, which experiences a kinematic pattern from homogeneity to heterogeneity in space, as shown in Figure 1. A single shear band is captured during the softening phase of deviatoric stress evolution.

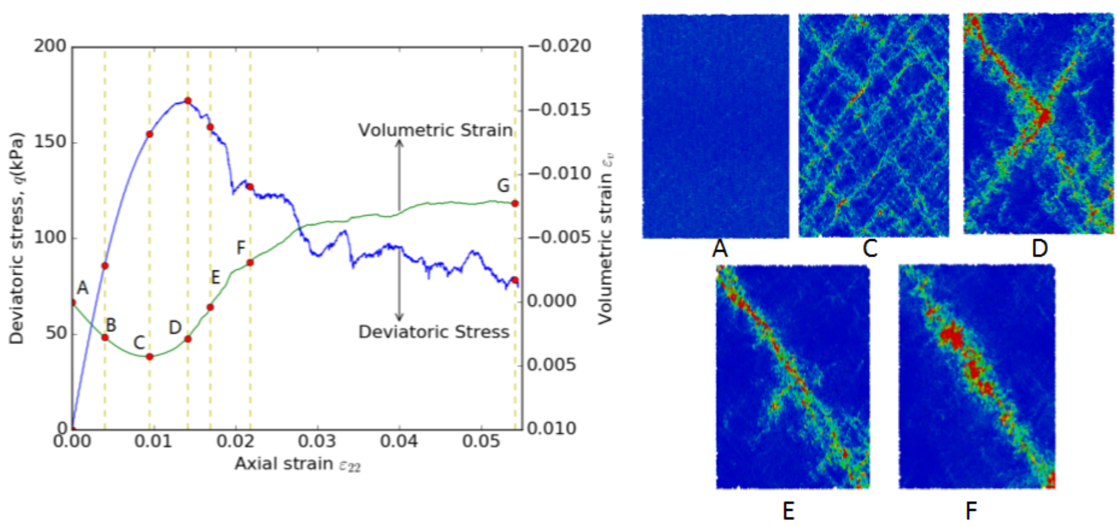

Figure 1. Stress-strain relation of a dense specimen under biaxial loading and the corresponding incremental strain field

From the initial state to the critical state, the bulk suffers from the buckling events of force chains, which is thought to induce the softening of deviatoric stress. The exchanges between different sizes of meso loops will contribute to anisotropy and volumetric changes. Two typical loop structures (L3 and L6, the number denotes the edge number of the polygons) are selected and their possible changes are shown in Figure 2.

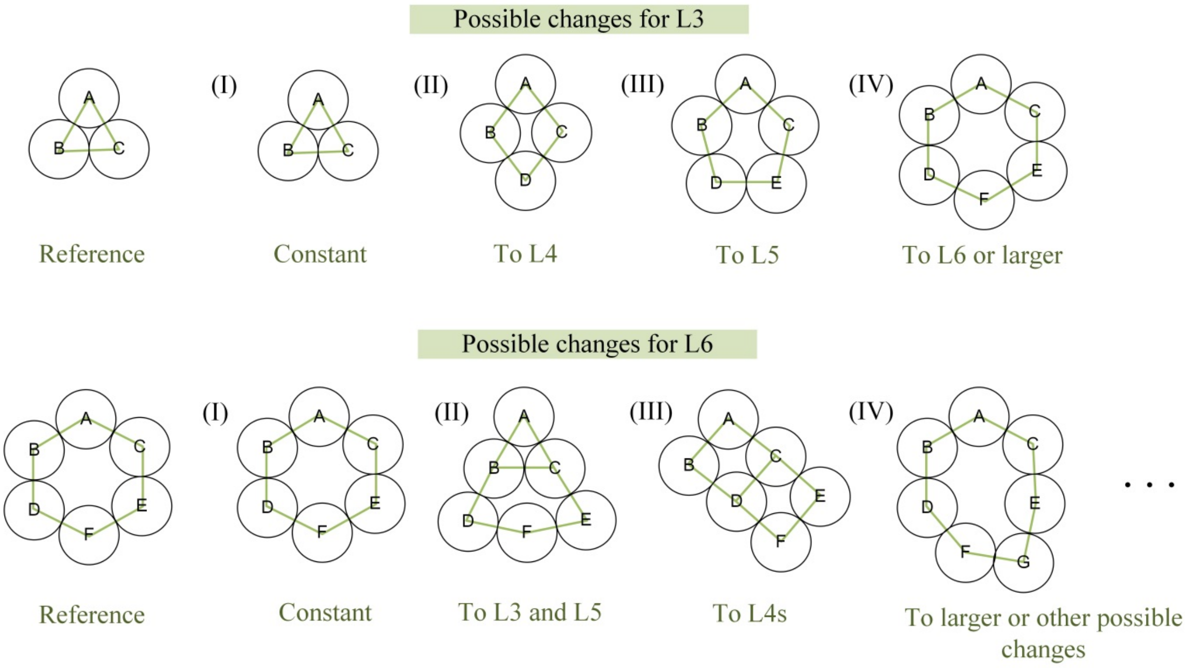

Figure 2. Possible changes for L3 and L6

The rough classification of these future changes is defined as follows: Future_3C, Future_3La, Future_3Lb, Future_6C, Future_6S and Future_6L. *C* represents the constant ones, *L* denotes that the cells become large and *S* means that the loops are shrinking; for L3, *La* means L3 changes to L4, and *Lb* means it changes to L5 or to larger ones. The evolution of these exchanges and the distributions are shown in Figure 3. The constant elements are decreasing while the newborns with a larger structure dominate the exchanges, and these transformations take place mainly inside the shear band.

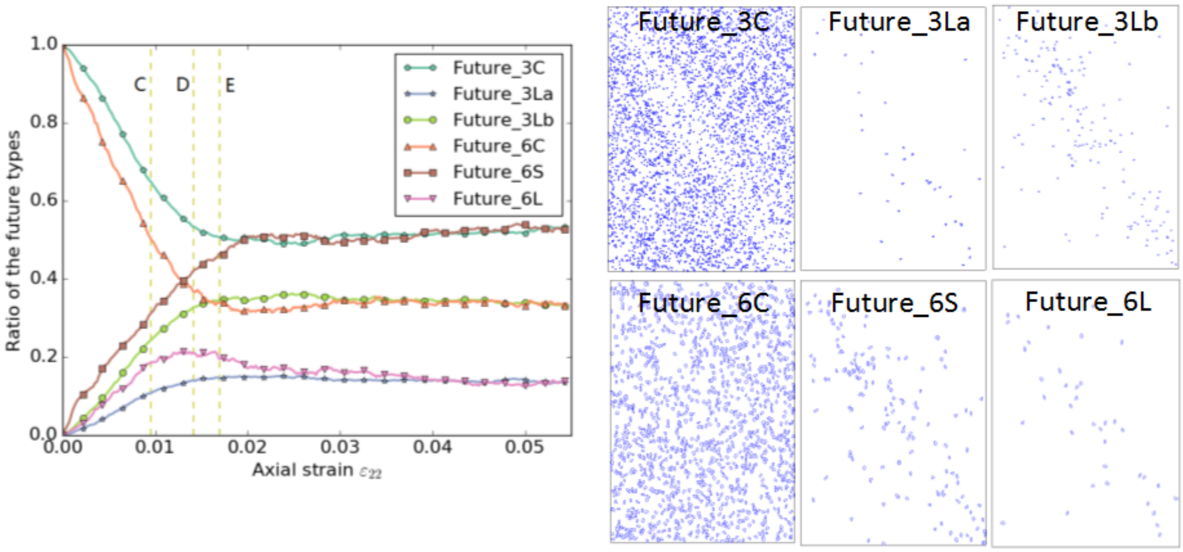

Figure 3. Evolutions of futures of L3 and L6 and the distribution at State F

References

Nicot, F. and Darve, F., 2011. Diffuse and localized failure modes: two competing mechanisms. *International Journal for Numerical and Analytical Methods in Geomechanics*, 35 (5), pp.586–601.

Nicot, F., Darve, F., 2007. A micro-mechanical investigation of bifurcation in granular materials. *International Journal of Solids and Structures*, 44 (20), pp. 6630–6652.

Nicot, F., Darve, F., Dat Vu Khoa, H., 2007. Bifurcation and second-order work in geomaterials. *International Journal for Numerical and Analytical Methods in Geomechanics*, 31 (8), pp.1007–1032.

Nguyen, N.-S., Magoariec, H. and Cambou, B., 2012. Local stress analysis in granular materials at a mesoscale. *International Journal for Numerical and Analytical Methods in Geomechanics*, 36 (14), pp.1609-1635.

Tordesillas, A., Muthuswamy, M., Walsh, S. D., 2008. Mesoscale measures of nonaffine deformation in dense granular assemblies. *Journal of Engineering Mechanics*, 134 (12), pp.1095–1113.

Zhu, H., Nicot, F. and Darve, F., 2016a. Meso-structure organization in two-dimensional granular materials along biaxial loading path. *International Journal of Solids and Structures* 96, pp. 25–37.

Zhu, H., Nguyen, H. N., Nicot, F. and Darve, F., 2016b. On a common critical state in localized and diffuse failure modes. *Journal of the Mechanics and Physics of Solids* 95, pp.112–131.

Chemo-mechanical processes at the pore scale: new insights from the pore scale

A. Lassin[1]*, F. Osselin[2,3], T. Fen-Chong[2], A. Fabbri[4], L. Mercury[5,6] & M. Azaroual[1,6]

[1]*BRGM, Orléans, France*
[2]*Institut Navier-IFSTTAR, Champs-sur-Marne, France*
[3]*Universty of Calgary, Canada (present address)*
[4]*ENTPE, Villeurbanne, France*
[5]*University of Orléans, France*
[6]*UMR ISTO 7327, Orléans, France*
**a.lassin@brgm.fr*

Coupled chemical and mechanical processes take place in numerous contexts related to geosciences and can concern human activities, such as the geological storage of CO_2 in deep saline aquifers. They mostly occur at the pore scale but may have consequences at larger scales. The processes of concern are crystallization pressure, capillary pressure, and pressure solution. The aim of this presentation is to show case studies of such processes, including experimental and theoretical approaches. It also aims to indicate the similarities between the various processes.

Crystallization pressure is known especially in the context of the alteration of building materials (Scherer, 2004): when a porous material is in contact with an aqueous solution (e.g., ground water) and subject to evaporation, capillary rise will conduct dissolved matter inside the porosity of the material. Evaporation concentrates the pore solution up to saturation with the solid salts. Then, if transport is faster than evaporation, salt precipitation will occur at the surface of the material. This phenomenon is called efflorescence and is not so damaging. On the other hand, if evaporation is faster than transport, for example at the top of the capillary rise, salt precipitation will occur inside the porosity. This phenomenon, called subflorescence, can provoke significant damage to the material due to the set-up of an excess pressure between the pore walls and the surface of the growing salt crystals. This excess pressure, called the disjoining pressure, is related to the super-saturation of the pore solution with respect to the salt solubility and the constrained curvature of the salt crystal because of the geometrical confinement imposed by the pore wall (Steiger, 2005).

A recent study (Osselin and others, 2015, 2013) explored the context of CO_2 geological storage in order to identify the conditions which could favour the development of crystallization pressures and the resulting possible alteration of the physical properties of the reservoir rock. Indeed, injection of CO_2 in a deep saline aquifer is expected to dry out the near-wellbore region and provoke massive salt precipitations. Application of poromechanics to such a system showed two cases that could lead to the generation of crystallization pressure. The first one occurs at the early stages of the CO_2 injection during the evaporation of the residual water, after the immiscible displacement of the pore water pushed by the incoming supercritical CO_2. The second case occurs over a longer time scale, in a region where water partially saturates the porosity and is still hydraulically connected with the reservoir rock pore water. In this case, the continuous evaporation of water in the gas phase drains solutes towards the evaporation front where super-saturation with respect to salts can increase while the larger pores are already filled with salt crystals.

Capillary pressure also occurs in partially water-saturated porous media, where the local relative humidity is particularly low. In such conditions, the radius of the menisci at the air-water interface is so small that the pressure in the liquid phase is strongly negative, in accordance with the Young-Laplace law. Consequently, the thermodynamic properties of water, solutes and eventually minerals are different compared to the saturated conditions. This means that the chemical equilibria are shifted and thus generate driving forces that can trigger chemical reactions. Field observations made in lateritic profiles by Tardy and Novikoff (1988) suggest such behaviours: hydrated minerals are preferentially observed in large pores, which can be filled with water only when the humidity is high; less hydrated minerals are rather observed in small pores, which can remain saturated with water when the relative humidity is low (*i.e.* dry conditions). This effect can be formally described by considering capillary pressure (Lassin, Azaroual, and Mercury, 2005). Experimental studies have been carried out in order to further investigate the phenomenon, showing figures of dissolution/re-precipitation of salts in synthetic pores or capillaries (Bouzid *et al*., 2011a,b, Shmulovich *et al*., 2009) or enhanced gas solubility in natural finely porous media (Lassin *et al*., 2016). In some instances change in reactivity can be enhanced by the set-up of anisobaric configurations, namely when capillary water and the mineral in contact are not at the same pressure.

The third phenomenon evoked is the pressure solution. It takes place in porous geological environments where the lithostatic load exerts a strong pressure at the contact between the solid grains of the rock while the pore water is at the hydrostatic pressure. A typical example is the formation of stylolites during diagenesis: dissolution occurs at the grain-grain contact and re-precipitation takes place on the neighbouring unconstrained grain surface. This results in the compaction of the rock and the decrease of the porosity (Passchier and Trouw, 1996). The phenomenon is complex and several models exist for describing the contact zone (Anzalone *et al*., 2006, Zhang and Spiers, 2005) but, in any case, anisobary is involved as in capillary phenomena. In addition, a link between pressure solution and crystallization pressure can be highlighted. Indeed, as pointed out by Dysthe (2014) these two phenomena are inverse processes: the latter occurs in a context of growing minerals whereas the former accompanies mineral dissolution. However both mechanisms require the existence of a liquid film between solids so that the excess stress exerted by the disjoining pressure and the transport of solutes can take place. According to Dysthe (2014), the largest driving force behind these two phenomena is linear in stress and of several orders of magnitude greater than other contributions that rather affect the kinetics of the process.

In conclusion, it can be said that coupled chemo-mechanical phenomena can take place in many environments and can be triggered by either chemical or mechanical constraints. Theoretical developments and the poromechanical approach, in particular, are able to explain the main features of these coupled phenomena. However, it seems that no simulation tool able to implement the numerical modelling of realistic systems that include coupled hydro-chemo-mechanical (and eventually thermal) processes exist. The development of such a tool, through collaborative projects involving the specialists of the different domains, would greatly contribute to realising the applications in the domains of CO_2 geological storage or of geothermal energy production, amongst others.

References

Anzalone, A., Boles, J., Greene, G., Young, K., Israelachvili, J., and Alcantar, N., 2006. Confined fluids and their role in pressure solution: Chemical Geology, 230, pp. 220-231.

Bouzid, M., Mercury, L., Lassin, A., and Matray, J.-M., 2011a. Salt precipitation and trapped liquid cavitation in micrometric capillary tubes. *Journal of Colloid and Interface Science*, 360, pp. 768-776.

Bouzid, M., Mercury, L., Lassin, A., Matray, J.-M., and Azaroual, M., 2011b. In-pore tensile stress by drying-induced capillary bridges inside porous materials. *Journal of Colloid and Interface Science*, 355, pp. 494-502.

Dysthe, D. K., 2014. Shaping the Interface – Interactions Between Confined Water and the Confining Solid, *in* Mercury, L., Tas, N., and Zilberbrand, M., editors, Transport and Reactivity of Solutions in Confined Hydrosystems: Dordrecht, Springer Netherlands, pp. 199-212.

Lassin, A., Azaroual, M., and Mercury, L., 2005. Geochemistry of unsaturated soil systems: aqueous speciation and solubility of minerals and gases in capillary solutions. *Geochimica et Cosmochimica Acta*, 69, pp. 5187-5201.

Lassin, A., Marty, N. C. M., Gailhanou, H., Henry, B., Trémosa, J., Lerouge, C., Madé, B., Altmann, S., and Gaucher, E. C., 2016. Equilibrium partial pressure of CO_2 in Callovian–Oxfordian argillite as a function of relative humidity: Experiments and modelling. *Geochimica et Cosmochimica Acta*, 186, pp. 91-104.

Osselin, F., Fabbri, A., Fen-Chong, T., Dangla, P., Pereira, J.-M., and Lassin, A., 2015. Stress from NaCl crystallisation by carbon dioxide injection in aquifers. *Environmental Geotechnics*, 2, pp. 280-291.

Osselin, F., Fen-Chong, T., Fabbri, A., Lassin, A., Pereira, J.-M., and Dangla, P., 2013. Dependence on injection temperature and on aquifer's petrophysical properties of the local stress applying on the pore wall of a crystallized pore in the context of CO_2 storage in deep saline aquifers. *The European Physical Journal - Applied Physics*, 64, p. 21101.

Passchier, C. W., and Trouw, R. A. J., 1996. Micro-tectonics. Springer-Verlag, Berlin, Heidelberg, New-York, 289 p.

Scherer, G. W., 2004. Stress from crystallization of salt. *Cement and Concrete Research*, 34, pp. 1613-1624.

Shmulovich, K. I., Mercury, L., Thiéry, R., Ramboz, C., and El Mekki, M., 2009. Experimental superheating of water and aqueous solutions. *Geochimica et Cosmochimica Acta*, 73, pp. 2457-2470.

Steiger, M., 2005. Crystal growth in porous materials - II: Influence of crystal size on the crystallization pressure. *Journal of Crystal Growth*, 282, pp. 470-481.

Tardy, Y., and Novikoff, A., 1988. Activité de l'eau et déplacement des équilibres gibbsite-kaolinite dans les profils latéritiques. *Compte-rendus de l'Académie des Sciences, Paris*, 306 (série II), pp. 39-44.

Zhang, X., and Spiers, C. J., 2005. Effects of phosphate ions on intergranular pressure solution in calcite: An experimental study. *Geochimica et Cosmochimica Acta*, 69, pp. 5681-5691.

On the interface shearing behavior between granular soil and artificial rough surfaces

Wan-Huan Zhou*, Xueying Jing* and Huaxiang Zhu*

**Department of Civil and Environmental Engineering, University of Macau*
hannahzhou@umac.mo

The soil-structural interface (SSI) exists in a variety of engineering situations, such as pile engineering, soil nailing, and the ground improvement with geotextiles. The shearing behavior of SSI is one of the most significant properties in engineering design and numerical modeling of geotechnical engineering problems (Yin & Zhou 2009; Su et al. 2010; Zhou et al. 2011). Previous investigations have mainly relied on experimental approaches to characterize the mechanical behavior of the interface based on macroscopic observations (Uesugi & Kishida 1986; Hu & Pu 2005; DeJong et al. 2006; Zhang et al. 2006; Hossain & Yin 2014). However, these investigations failed to properly explain the micro-physical mechanisms of the shearing between the soil and structural interface. The interface was normally quantified as one parameter, most commonly, the relative roughness (R_n) proposed by Uesugi and Kishida (1986). In this presentation, 2D numerical interface shearing tests (Figure 1(a)) with a periodic boundary condition are performed in discrete element method (DEM) to investigate the shear-banding process and the evolution of soil fabric to the critical state in densely and loosely packed granular soils. A series of laboratory interface shear tests are conducted with different surface roughness of steel. Additionally, the shear behavior and the role of shear direction at the interface shearing (Figure 1(b)) are investigated at the macro-scale and particle scale using a series of 3D interface modeling tests conducted in DEM. The main conclusions are as follows:

(1) The degree of strain localization, quantified by a proposed new indicator, α, steadily ascends during the stress hardening regime, dramatically jumps prior to the stress peak, and stabilizes at the stress steady state (Zhu et al., 2017). Loose specimen does not develop a steady localized band at the large strain, as the deformation pattern transforms between localized and diffused failure modes. During the stress steady state of both specimens, remarkable correlations are observed between α and the shear stress, as well as between α and the volumetric strain rate (Figure 2). Disregarding different initial void ratios, a common critical state micro-structure is beheld in large shear deformation of the soil with generally the same fabric arrangement in terms of both the contacts' orientation and the internal force transmission. Due to systematic forming, buckling and the collapse of force-chains, an angular zone (called α-zone), within which the contact density varies sluggishly, appears and extends around the major direction of the distribution of contact orientation inside the localized band.

(2) The 3D interface modeling tests show that a localized band with intense shear deformation emerges from the contact plane and expands gradually as shearing progresses before stabilizing at the residual stress state. The thickness of the localized band is affected by the normalized roughness of the interface and the normal stress, varying between 4 and 5 times the median grain diameter (Jing et al., 2017.), as shown in Figure 3. A thicker localized band is formed when the soil has a rough shearing interface. After the appearance of the localized band, the granular material structuralizes into two regions: the interface zone and

the upper zone. The mechanical behavior in the interface zone is representative of the interface according to the local average stress analysis.

(3) When the shear direction is orthogonal to the surface's roughness anisotropy direction (SRAD), the shear resistance of the soil has been completely mobilized, leading to the maximum shear strength and maximum thickness of the localized band. When the shear direction is parallel to the SRAD, the shear resistance is the minimum and no obvious localized band formed. The volumetric strain responses in the interface shearing tests principally originate from the change of porosity within the localized banding domain during shearing.

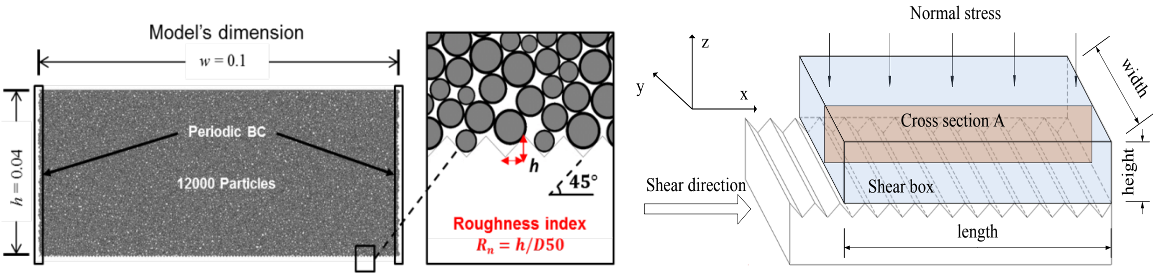

(a) (b)

Figure 1. Schematic diagram of the interface shear apparatus: (a) 2D modelling; (b) 3D modelling

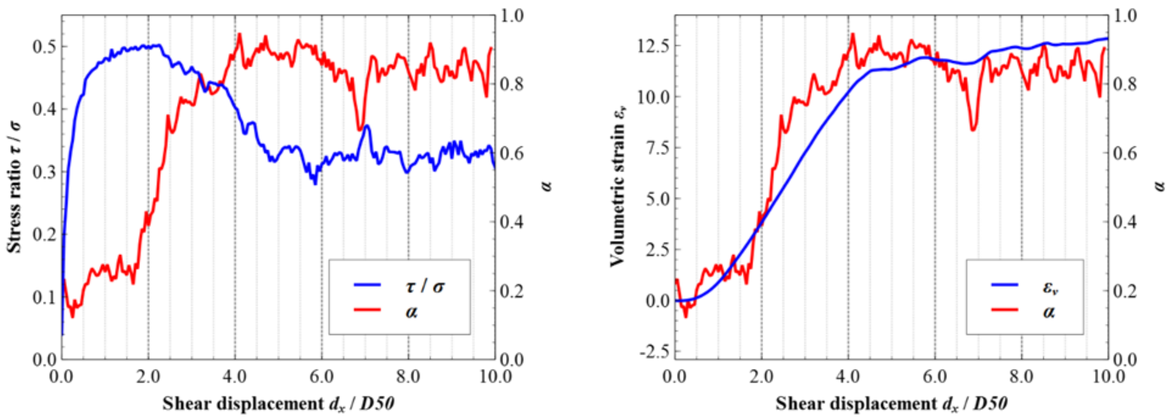

(a) (b)

Figure 2. Correlations between the degree of the strain localization α and the shear behavior: (a) α and shear stress; (b) α and Volumetric strain

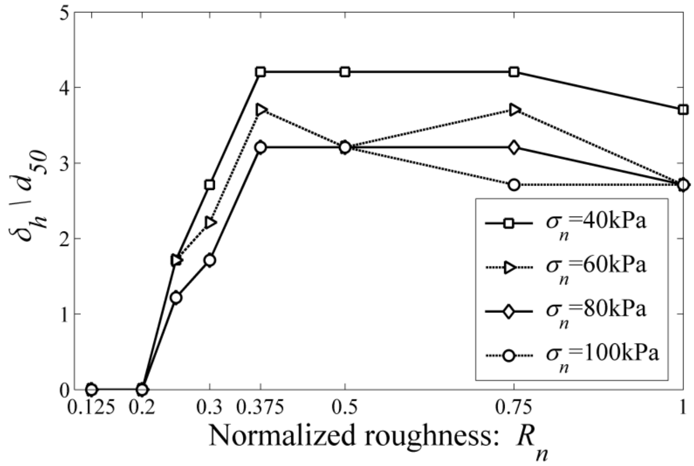

Figure 3. Normalized thickness of the interface zone δ_h/d_{50} as a function of normalized roughness R_n under various normal stress σ_n.

References

DeJong, J.T., White, D.J. & Randolph, M.F., 2006. Microscale observation and modeling of soil-structure interface behavior using particle image. *Soils and Foundations*, 46(1), pp.15–28.

Jing XY, Zhou WH, Zhu HX, Yin ZY. and Li YM. 2017. Analysis of soil-structural interface behavior using three-dimensional DEM simulations, *Int J Numer Anal Methods Geomech*. 2017; 1–19. DOI:10.1002/nag.2745.

Hossain, M.A. & Yin, J.H., 2014. Behavior of a Pressure-Grouted Soil-Cement Interface in Direct Shear Tests. *International Journal of Geomechanics*, 14(1), pp.101–109.

Hu, L.M. & Pu, J.L., 2005. Testing and Modeling of soil-structure Interface. *Journal of Geotechnical and Geoenvironmental Engineering*, 130(8), pp.851–860.

Su, L.J., Yin, J.H. & Zhou, W.H., 2010. Influences of overburden pressure and soil dilation on soil nail pull-out resistance. *Computers and Geotechnics*, 37(4), pp.555–564.

Uesugi, M. & Kishida, H., 1986. Frictional resistance at yield between dry sand and mild steel. *Soils and Foundations*, 26(4), pp.139–149.

Yin, J.H. & Zhou, W.H., 2009. Influence of grouting pressure and overburden stress on the interface resistance of a soil nail. *Journal of Geotechnical and Geoenvironmental Engineering*, 135(9), pp.1198–1208.

Zhang, G., Liang, D.F. & Zhang, J.M., 2006. Image analysis measurement of soil particle movement during a soil-structure interface test. *Computers and Geotechnics*, 33(4-5), pp.248–259.

Zhou, W.H., Yin, J.H. & Hong, C.Y., 2011. Finite Element Modelling of Pullout Testing on a Soil Nail in a Pullout Box Under Different Overburden and Grouting Pressures. *Canadian Geotechnical Journal*, 48(4), pp.557–567.

Zhu H., Zhou W.H., Yin Z.Y., 2017. Deformation mechanism of strain localization in 2D numerical interface tests, *Acta Geotechnica*. In press. DOI: 10.1007/s11440-017-0561-1.

Micro-inertia origin of instabilities in dry granular materials

A. Wautier[1,2,3], S. Bonelli[2] & F. Nicot[3]

[1]AgroParisTech-ENGREF, 19 avenue du Maine, 75732 Paris, France.
[2] Irstea UR RECOVER, 3275 Rte Cézanne, CS 40061, 13182 Aix-en-Provence Cedex 5, France.
[3]Université Grenoble Alpes, Irstea, UR ETGR, 2 rue de la Papeterie BP 76, F-38402 St-Martin-d'Hères, France.
antoine.wautier@irstea.fr

Based on the concept of the second-order work criterion introduced by Hill (Hill, 1958), recent papers have demonstrated the ability of this criterion to predict the occurrence of material instabilities characterized by an outburst of kinetic energy. In particular, it has been shown that the vanishing of the second order work is a necessary condition for the existence of instabilities of any type (Nicot et al., 2009; Daouadji et al., 2011; Wan et al., 2013). Within the framework of small strain continuum mechanics, Hill's instability criterion, applied to a material point, states that for a given equilibrium $(\boldsymbol{\sigma};\boldsymbol{\varepsilon})$ reached after a given loading history, if there exists at least one stress increment $\mathbf{d}\boldsymbol{\sigma}$ associated with a strain response $\mathbf{d}\boldsymbol{\varepsilon}$ such that $W_2 = \mathbf{d}\boldsymbol{\sigma} : \mathbf{d}\boldsymbol{\varepsilon} < 0$, the material point is unstable. The physical meaning of the vanishing of the second order work (W_2) corresponds to a situation in which the deformation of the mechanical system can be pursued without any input of energy from the observer. However not every loading program will necessarily trigger off this underlying instability.

Sample preparation and numerical testing

Thanks to the use of the YADE software, a cubic assembly of 10,000 spherical particles is generated following a uniformly distributed particle size distribution such that $r_{\max} = 3.5\, r_{\min}$. At the microscale, the interactions between grains are modelled thanks to a classical elasto-frictional contact law with parameters given in Table below.

Parameters	Value
Density	3,000 kg.m-3
Young Modulus (E)	356 MPa
Stiffness ratio (ν)	0.42
Inter-particle friction angle (φ)	35°
Particle-wall friction angle	0°
Number of particles	10,000

A loose sample with a void ratio of 0.73 is prepared following the radius expansion technique and then submitted to a drained triaxial under a confining pressure of 100 kPa up to a stress ratio $q/p = 0.45$. For this mechanical stress state, a directional analysis performed in Rendulic's plane (Sibille et al., 2009; Nicot et al., 2009) demonstrates that our sample is at a bifurcation point characterized by the vanishing of the second order work for some loading directions (see Figure 1).

For a particular unstable loading direction characterized by an angle $\theta = 210°$ in Rendulic's plane, the time response of the specimen is studied from a micromechanical point of view in order to highlight the underlying mechanisms leading to the vanishing of W_2. In Figure 1, the particle kinetic energy is shown while an incremental loading of $||\mathbf{d}\boldsymbol{\sigma}|| = 5$ kPa is applied in the form of a ramp.

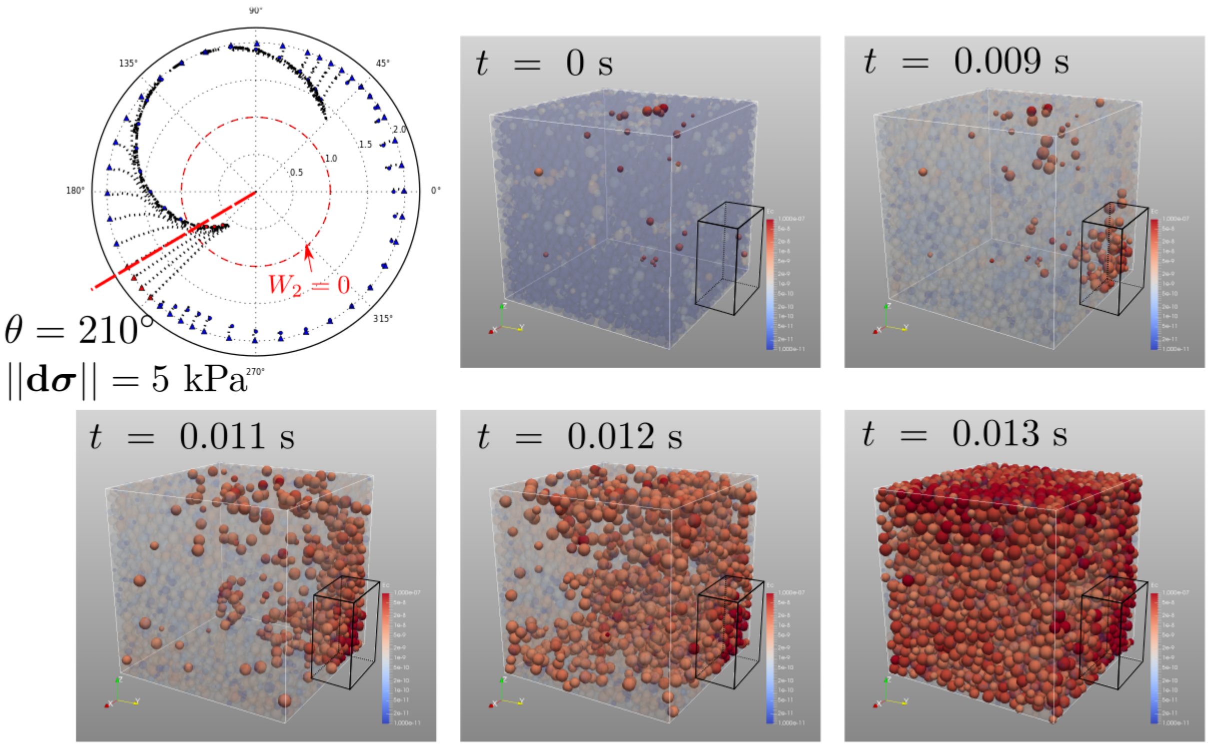

Figure 1: Macroscopic second order work envelope in Rendulic's plane (top left). Onset and propagation of the burst of kinetic energy for $\theta = 210.5°$ and an incremental stress perturbation $||d\sigma|| =$ 5 kPa. Particles with $E_c > 10^{-8}$ J are highlighted. A control volume around the location of the kinetic burst is shown in black.

A localized burst of kinetic energy appears in a zone materialized by a small control volume (in black in Figure 1) and propagates to the whole sample. In the case where no vanishing of W_2 is observed, the bursts of kinetic energy never propagate to the whole sample. As a result, an underlying instability requires a microstructure prone to reorganize as a whole, provided that a burst of kinetic energy is created by a change in the macroscopic loading conditions.

Mesoscale mechanisms leading to the vanishing of W_2

Based on a time analysis of the population of particles belonging to force chains (according to the definition proposed by Peters et al., 2005), it can be shown that the observed burst of kinetic energy appears prior to the destruction of the existing force chains. Indeed force chains are elongated column-like structures loaded in compression and their effective failure is very likely to be related to the onset of bending. Given a group of three chained particles from which two contact directions form an angle $\beta \in [0, \pi]$, a bsnding rate can be defined as $\dot{\beta}$. A force chain bends as long as $\dot{\beta} > 0$.

In Figure 2, the time evolution of the mean kinetic energy (left) and the mean bending rate (right) are shown for the whole sample and the small control volume around the location of the burst of kinetic energy (see Figure 1). In this Figure, the onset of the burst of kinetic energy and the increase in the bending rate in the control volume occur simultaneously prior to the general increase in kinetic energy and the bending rate for the whole sample. Indeed, the localized bending of a few force chains seems to be sufficient to generate a loss of controllability at the scale of the REV.

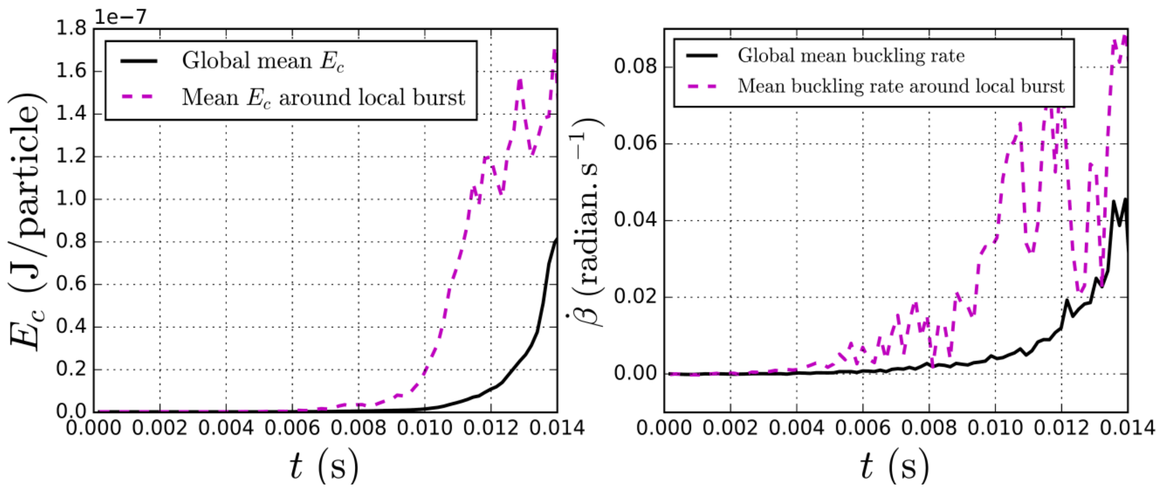

Figure 2: Mean kinetic energy per particle for the whole sample and close to initiation of the kinetic burst (left), mean bending rate of the groups of three chained particles for the whole sample and around the kinetic burst (right).

As recently shown in 2D (Tordesillas et al., 2011; Zhu et al., 2016), the force chain loss of stability results from the opening of contacting grain cycles. In order to investigate this feature in 3D, the time evolutions of the number of contacts between two chained particles (N_{cc}), two non-chained particles (N_{nn}) and a non-chained and a chained particle (N_{nc}) are represented in Figure 3. The onset and propagation of the burst of kinetic energy is shown by two solidly thick vertical lines.

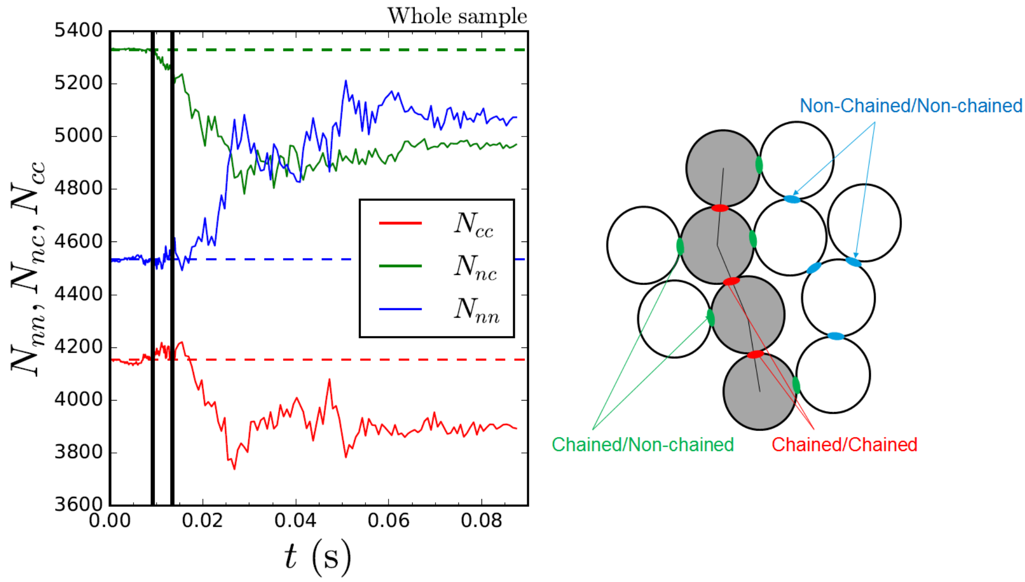

Figure 3: Time evolution of the number of contacts between two chained particles ($\boldsymbol{N_{cc}}$), two non-chained particles ($\boldsymbol{N_{nn}}$) and a non-chained and a chained particle ($\boldsymbol{N_{nc}}$). The onset and the propagation of the burst of kinetic energy is delimited by two vertical lines.

In Figure 3, an early decrease in chained/non-chained contacts can be seen, which tends to prove that the localized bending highlighted in Figure 2 results from an early unjamming of force chains (consequently, a local dilatancy).

Conclusion

Within the framework of the second order work theory, the onset of instabilities was explored numerically in granular materials through three dimensional DEM simulations. Stress controlled directional analysis were performed in Rendulic's plane and particular attention was paid to transient evolutions at the microscale. The onset and development of transient mechanical instabilities was shown to result from the unjamming and bending of a few force chains associated with a local burst of kinetic energy. This burst of kinetic energy propagates to the whole sample and provokes a generalized unjamming of force chains. As force chains bend, a phase transition from a quasi-static to an inertial regime has been observed.

References

Hill, R., 1958. A general theory of uniqueness and stability in elastic-plastic solids. *Journal of the Mechanics and Physics of Solids 6 (3)*, 236–249.

Daouadji, A., Darve, F., Al Gali, H., Hicher, P., Laouafa, F., Lignon, S., Nicot, F., Nova, R., Pinheiro, M., Prunier, F., et al., 2011. Diffuse failure in geomaterials: experiments, theory and modelling. *International Journal for Numerical and Analytical Methods in Geomechanics 35 (16)*, 1731–1773.

Nicot, F., Sibille, L., Darve, F., 2009. Bifurcation in granular materials: An attempt for a unified framework. *International Journal of Solids and Structures 46 (22),* 3938–3947.

Peters, J. F., Muthuswamy, M., Wibowo, J., Tordesillas, A., 2005. Characterization of force chains in granular material. *Physical Review E 72 (4),* 041307.

Sibille, L., Nicot, F., Donzé, F.-V., Darve, F., 2009. Analysis of failure occurrence from direct simulations. *European Journal of Environmental and Civil Engineering 13 (2),* 187–201.

Tordesillas, A., Lin, Q., Zhang, J., Behringer, R., Shi, J., 2011. Structural stability and jamming of self-organized cluster conformations in dense granular materials. *Journal of the Mechanics and Physics of Solids 59 (2)*, 265–296.

Wan, R., Pinheiro, M., Daouadji, A., Jrad, M., Darve, F., 2013. Diffuse instabilities with transition to localization in loose granular materials. *International Journal for Numerical and Analytical Methods in Geomechanics 37 (10)*, 1292–1311.

Zhu, H., Nicot, F., Darve, F., 2016b. Meso-structure organization in two-dimensional granular materials along biaxial loading path. *International Journal of Solids and Structures 96*, 25–37.

Physical modelling of erosion with artificial cemented granular geomaterials

P. Philippe*, F. Brunier-Coulin*, Z. Benseghier*, L.-H. Luu*, P. Cuéllar, J.-Y. Delenne*** & S. Bonelli***

**IRSTEA, RECOVER Unit Research, Aix-en-Provence, France*
*** BAM, Division 7.2 Buildings and Structures, Berlin, Germany*
**** UMR IATE, INRA/CIRAD/Montpellier SupAgro, Montpellier, France.*
pierre.philippe@irstea.fr

The present presentation proposes and illustrates both experimental and numerical methods dedicated to physical modelling of cemented soil in the more general context of fluid flow surface erosion. For this purpose, artificial cemented granular systems have been developed, constituted of spherical particles bonded to each other by solid bridges having variable yield strength (Figure 1). Experimental traction tests at both grains contact and sample scales allowed for the cementation strength to be quantified while some impinging jet erosion tests on transparent systems (coupling refractive index matching and planar laser induced fluorescence) helped to identify the erosion threshold that can be satisfactorily predicted by a generalized Shields criterion. From the numerical point of view, a 2D DEM-LBM simulation was developed (Cuéllar 2015) and allowed both fluid/grains interactions to be properly described at the microscale and cohesion to be modelled by a contact law with a parabolic yield envelope including critical values in traction, shear and rolling (Delenne 2004).

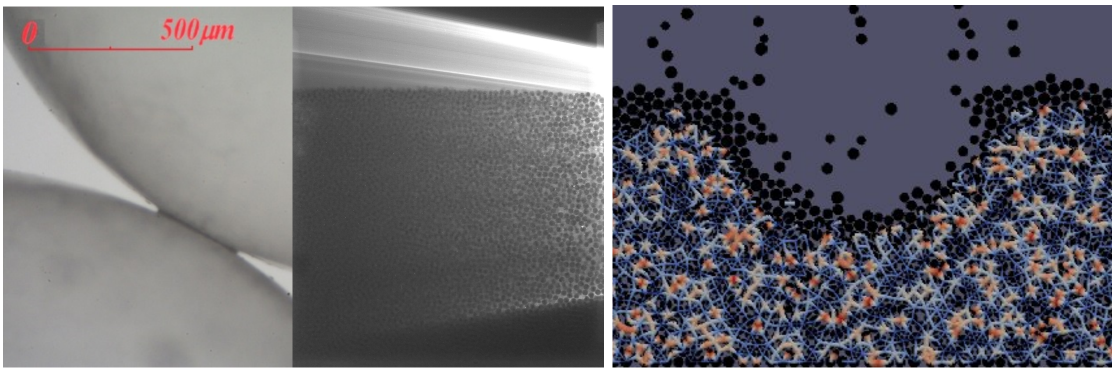

Figure 1. Illustrations of the different methodologies: (a) solid bonds; (b) Refractive Index Matching and Planar Laser Induced Fluorescence; (c) JET erosion by DEM-LBM modelling.

References

Cuéllar, P., Philippe, P., Bonelli, S., Benahmed, N., Brunier-Coulin, F., Ngoma, J., Delenne, J. Y. and Radjai, F., 2015. Micromechanical analysis of the surface erosion of a cohesive soil by means of a coupled LBM-DEM model. In: *PARTICLE-BASED METHODS IV-Fundamentals and Applications*, pp. 519-528.

Delenne, J. Y., El Youssoufi, M. S., Cherblanc, F. and Bénet, J. C., 2004. Mechanical behaviour and failure of cohesive granular materials. *International Journal for Numerical and Analytical Methods for Geomechanics*, 28, pp. 1577–1594.

Existence of an effective stress variable for quasi-elastic behaviour: new micromechanical evidences

J. Duriez* & R. Wan*

* *Department of Civil Engineering, University of Calgary*
jerome.duriez@ucalgary.ca

Micromechanical approaches to granular materials are presented to discuss extension of the dry-state failure criterion and constitutive relations to unsaturated conditions through the effective stress concept. Namely, the contact stress σ_{ij}^{cont} that stems from intergranular contact forces f_i is isolated from the total stress of unsaturated materials, and tested as an effective stress candidate along various loading paths for dense and loose granular packings.

Because the direct expression of σ_{ij}^{cont} requires the knowledge of the contact force network, as per Eq. (1), i.e.

$$\boldsymbol{\sigma_{ij}^{cont}} = \frac{\mathbf{1}}{\mathbf{V}} \sum\nolimits_{\boldsymbol{cont.}} \boldsymbol{f_i}\, \boldsymbol{l_j} \qquad (1)$$

and since experimentally measuring the latter is an elusive task, a so-called µUNSAT expression is proposed in order to circumvent the need for such contact force measurements. Instead, the µUNSAT Eq. (2) provides an equivalent contact stress expression in terms of the total stress Σ_{ij}, the air and water pressures u_a and u_w with the corresponding suction $s = u_a - u_w$, the air-water surface tension γ and tensorial terms pertaining to the microstructures of the wetted solid surface S_w, of the air-water interface S_{aw}, and of the contour Γ, where the three phases meet (Chateau & Dormieux, 1995 ; Duriez & Wan, 2016, 2017; Duriez et al., 2017):

$$\sigma_{ij}^{cont} = \Sigma_{ij} - u_a\delta_{ij} + \frac{1}{V}\left[s\left(V_w\,\delta_{ij} + \int_{S_w} n_i x_j dS\right) + \gamma\left(\int_{S_{aw}} (\delta_{ij} - n_i n_j) dS + \int_{\Gamma} \nu_i x_j dl\right)\right] \qquad (2)$$

with V_w the water volume; n_i the outwards normal to S_w or S_{aw}; x_i the position from the grains centroids of any point along the grain surfaces; and ν_i the tangent to S_{aw} being orthogonal to Γ. Clear formal discrepancies appear between the µUNSAT Eq. (2) and Bishop's equation.

Considering a Discrete Element Method model of wet granular material (Duriez & Wan, 2017b), the contact stress is then measured using Eq. (2) and its constitutive role assessed during triaxial compression, with the direction '1' serving as the axis of symmetry and '2,3' being the two other directions.

It is first recalled that the contact stress is a proper stress-strength effective stress in that the contact stress limit states in both dry and wet conditions conform with the same cohesionless Mohr Coulomb line, as opposed to the classically observed discrepancy in terms of total stress (Wan et al., 2015; Duriez & Wan, 2017b; Wan & Duriez, 2017).

As for the stress-strain constitutive behaviour, an investigation is conducted whereby exactly the same strain paths in dry and wet conditions are considered, while measuring the resulting contact stress. To do so, a classical triaxial compression $(d\varepsilon_1 = cst; d\Sigma_3 = 0)$ is first imposed on wet samples. The corresponding strain path is then directly applied as a strain-controlled loading path on similar dry samples. The objective of following the same strain paths in dry and wet conditions is to find out whether the obtained contact stress path is unique, which would mean that the latter relates to the former through a unique constitutive relation, whatever the saturation is, and would establish a complete stress-strain effective stress framework.

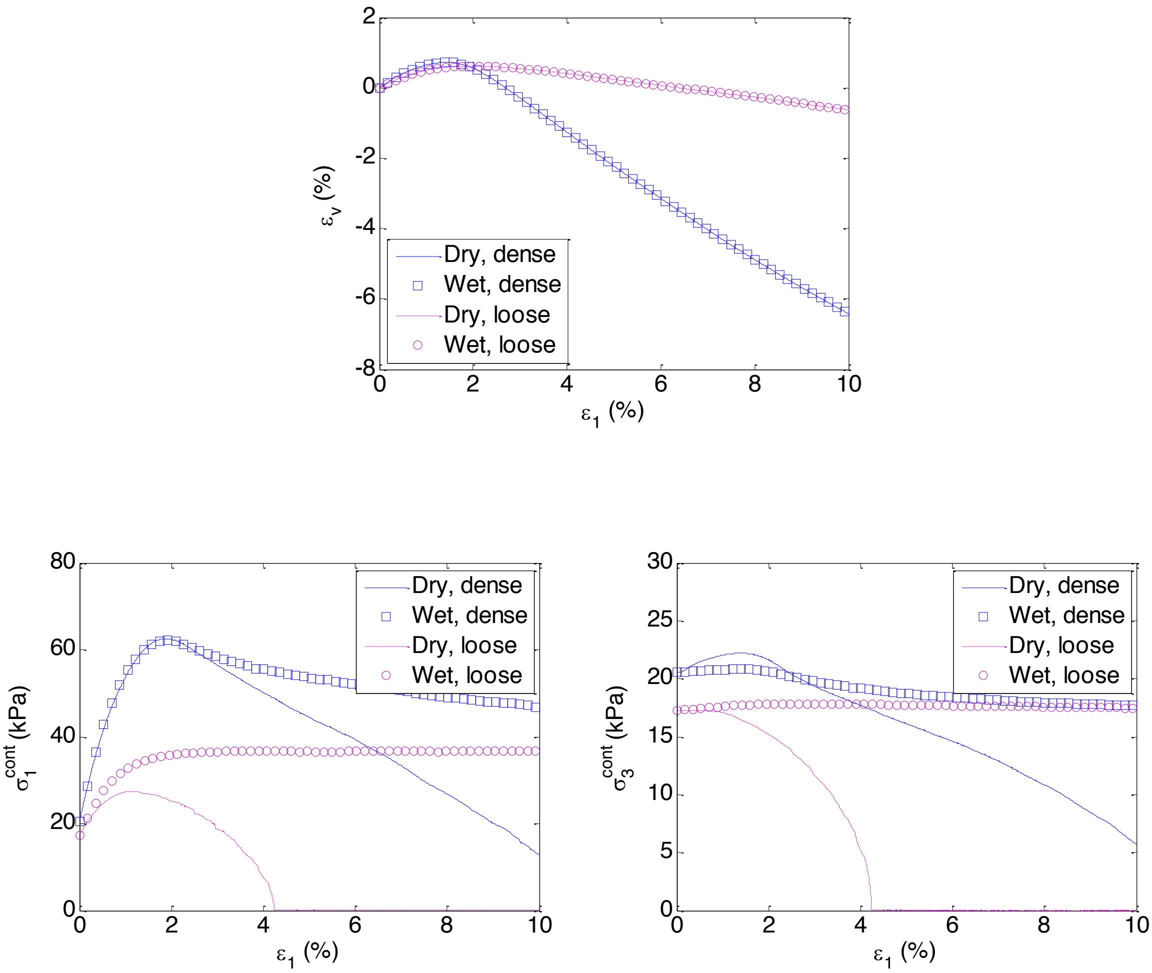

Figure 1. Stress-strain effective nature of the contact stress for dense or loose granular material: dry-wet comparison of contact stress responses (bottom) to the same strain path (top) (Duriez et al., 2017b)

Dry-wet comparisons (Figure 1) actually reveal unique contact stress responses in limited quasi-elastic domains that are restricted to the pre-peak phase for dense packings, and to the initial stiffnesses for the loose packings. Under those restrictions, it is demonstrated that dry-state constitutive relations used together with the contact stress are adequate to predict the strains in unsaturated conditions, which provides a connection to the principle of effective stress.

The uniqueness of the constitutive relation for all saturations together with the stress-strain effective nature of the contact stress are subsequently lost once interparticle sliding is fully mobilized in the elasto-plastic regime (Duriez et al., 2017b).

References

Chateau, X. and Dormieux, L., 1995. Homogenization of a non-saturated porous medium: Hill's lemma and applications. *Comptes Rendus de l'Académie des Sciences*, 320:II, pp. 627-634.

Duriez J., Wan R., 2016. Stress in wet granular media with interfaces via homogenization and discrete element approaches. *Journal of Engineering Mechanics*, 142(12), pp. 04016099-1–9.

Duriez, J. and Wan, R., 2017. Subtleties in Discrete Element Modelling of wet granular soils. *Géotechnique*, 42(14), pp. 4258-4277.

Duriez, J. and Wan, R., 2017b. Contact angle mechanical influence for wet granular soils. *Acta Geotechnica*, 12(1), pp. 67-83.

Duriez, J., Eghbalian, M., Wan, R. and Darve, F., 2017. The micromechanical nature of stresses in triphasic granular media with interfaces. *Journal of the Mechanics and Physics of Solids*, 99, pp. 495-511.

Duriez, J., Wan, R. and Pouragha M., 2017b. Partially Saturated Granular Materials: Insights From Micro-Mechanical Modelling. In *Proceedings of the 6th Biot Conference*, Paris, July 2017.

Wan, R., Duriez, J. and Darve, F., 2015. A tensorial description of stresses in triphasic granular materials with interfaces. *Geomechanics for Energy and the Environment*, 4, pp. 73-87.

Wan, R. and Duriez, J., 2017. Micromechanical aspects of partially saturated granular media with reference to capillary and effective stresses. In *GdRI Geomech Workshop*, Nantes, January 2017

Grading-dependent behavior of granular material: from experiments to modelling

Zhen-Yu Yin*

**Research Institute of Civil Engineering and Mechanics (GeM), UMR CNRS 6183, Ecole Centrale de Nantes, Nantes 44321, France; Key Laboratory of Geotechnical and Underground Engineering of Ministry of Education, Tongji University, Shanghai 200092, China*

Email address: zhenyu.yin@ec-nantes.fr; zhenyu.yin@gmail.com

Natural soils or man-made fills are often mixtures of fine and coarse grains with a grain size distribution for a selected area. The proportions of these fine and coarse grains can change with time due to grain breakage or internal erosion. This phenomenon has a crucial effect on the safety of geotechnical structures. Therefore, the grading-dependent stress–strain behavior of granular materials needs to be better understood.

In general, the grain size distribution can be simplified as shown in Fig. 1 controlled by the maximum grain size, fines content f_c and slopes α and β. The grading change can be induced by the grain breakage with a decrease of α, or induced by the internal erosion with a decrease of f_c. Both phenomena can also cause the change of β. Therefore, f_c, α and β vary kinematically throughout the mechanical or/and hydraulic loading process, resulting in strength degradation and greater deformability for soils.

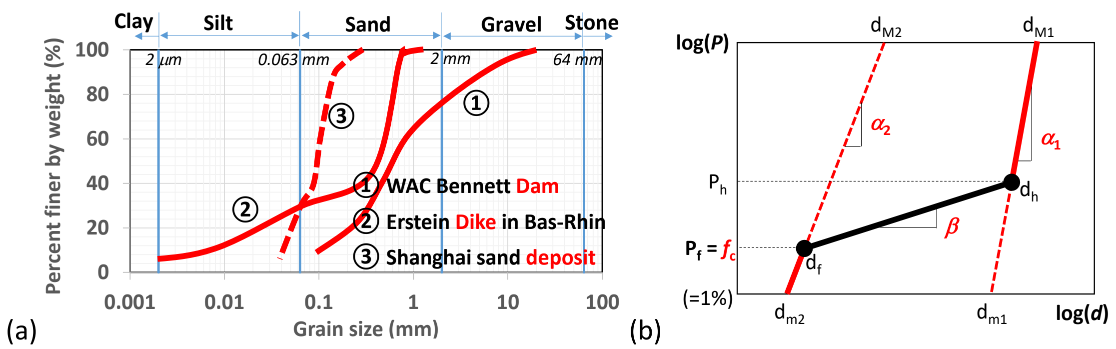

Fig. 1 Grain size distribution of (a) natural soils and man-made fills, and (b) simplified description

For a full coupling of mechanical or/and hydraulic loading process, an easily useful model with a simulation platform for a given GSD and a unified description of GSD-dependent mechanical responses are required.

A critical state based elastoplastic model (SIMSAND by Yin et al. (2013), Jin et al. (2016), shown in Fig. 2) with its implementation into a large deformation analysis in finite element code was first introduced, and then validated by extending the phenomena from laboratory mechanical behaviors to granular flows.

A series of drained and undrained triaxial tests were then carried out with three different materials (idealized spheres by DEM, glass balls and Hostun sand, see Liu et al., 2014). For each material, samples with different gradings and similar relative densities were prepared. Experimental results show that the friction strength is more or less independent of the grading (the coefficient of uniformity from 1.1 to 20). However, the position of the critical state line in the e-p' plane was significantly influenced by the grading (Fig. 3), based on which an exponential relationship was proposed between the reference critical void ratio and the uniformity coefficient or the slope α.

$$e_{ref} = e_{refu} + \left(e_{ref0} - e_{refu}\right) e^{-a(C_u - 1)} \tag{1}$$

The Eq. was validated to combine with the SIMSAND model to describe the regular grading-dependent mechanical behavior of granular materials, and further applied to the numerical modeling of sand with consideration to the effect of grain breakage (Yin et al., 2017).

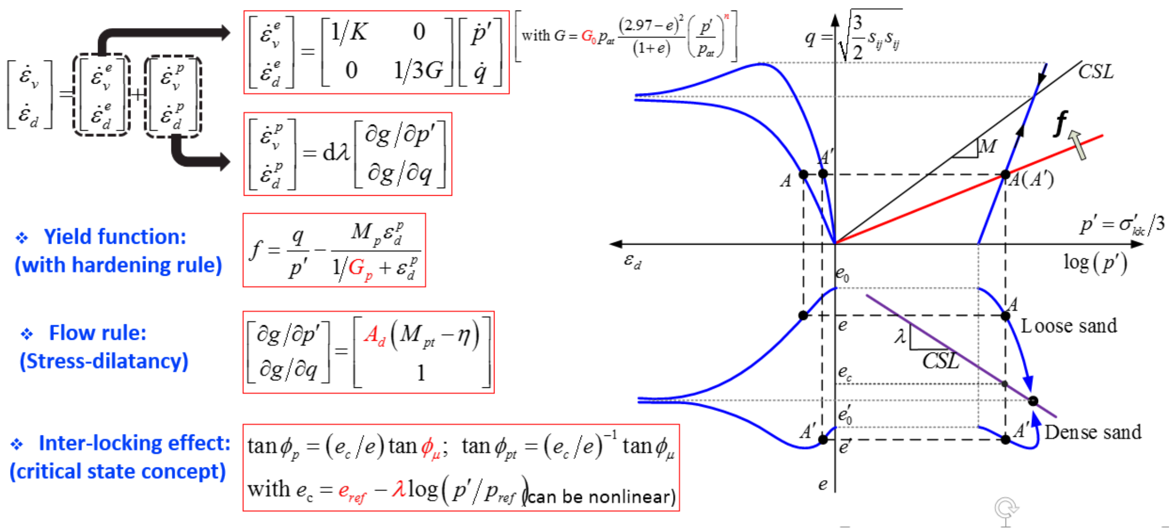

Fig. 2 Key constitutive equations and principle of the SIMSAND model

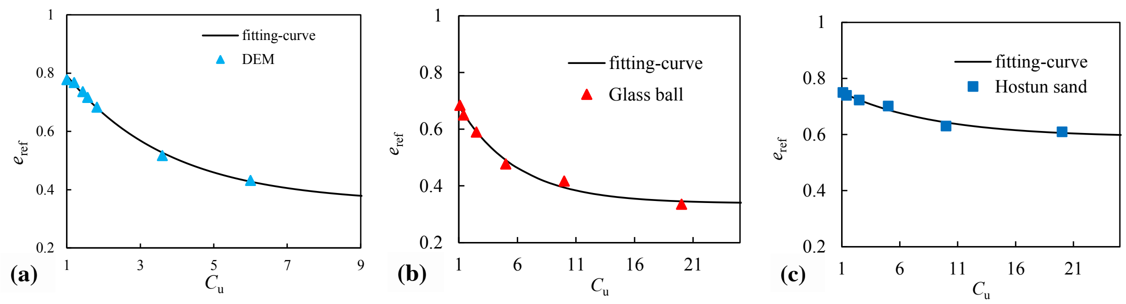

Fig. 3 The reference critical void ratio versus the uniformity coefficient for (a) idealized spheres by DEM, (b) glass balls and (c) Hostun sand

As for the effect of the fines content, experimental observations have shown the significant impact of fines or coarse grains on the behavior of sand-silt mixtures. The inter-grain contact index is firstly reviewed. A formulation which links the inter-grain contact index with the void ratio is then proposed and validated by measuring the index void ratios of various sand–silt mixtures. The formulation is applied to determine the position of the critical state line of sand–silt mixtures from sand to silt (see Fig. 4).

$$e_{ref}=\left[e_{hc,ref}\left(1-f_c\right)+af_c\right]\frac{1-\tanh\left[\xi\left(f_c-f_{th}\right)\right]}{2}+e_{hf,ref}\left(f_c+\frac{1-f_c}{\left(R_d\right)^m}\right)\frac{1+\tanh\left[\xi\left(f_c-f_{th}\right)\right]}{2} \tag{2}$$

Combining this formulation with the SIMSAND model, the modeling of the mechanical behavior of sand–silt mixtures from sand to silt was unified (Yin et al., 2014, 2016). The model was applied and validated to multiphysics modeling of internal erosion.

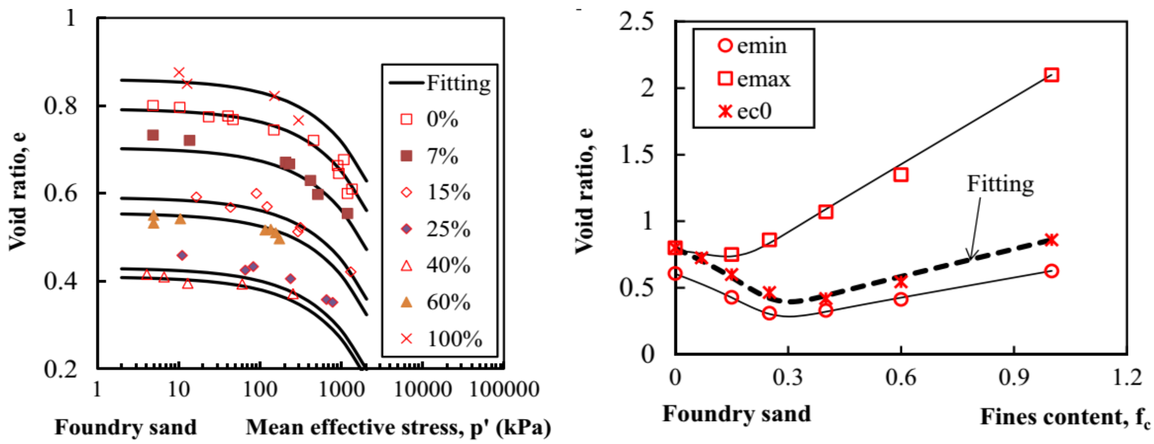

Fig. 4 Effect of fines content based on tests of Foundry sand-silt mixture for (a) critical state lines on e-p' plane and (b) index void ratio and reference critical void ratio

Finally the effect of the slope β was investigated by a two-dimensional discrete element method with a formulation of the reference critical state line. Further development of the method needs the support of experimental studies.

$$e_{ref}=a\beta^2+b\beta+c \tag{3}$$

Any ideas of how to unify the description for grading-dependency with f_c, α and β is open for discussion.

References

Jin, Y. F., Yin, Z. Y., Shen, S. L. and Hicher, P. Y., 2016. Investigation into MOGA for identifying parameters of a critical state based sand model and parameters correlation by factor analysis. *Acta Geotechnica*, 11(5), pp. 1131-1145.

Liu, Y. J., Li, G., Yin, Z. Y., Dano, C., Hicher, P. Y., Xia, X. H. and Wang, J. H., 2014. Influence of grading on undrained behavior of granular materials. *Comptes rendus Mecanique*, 342, pp. 85-95.

Yin, Z. Y., Xu, Q. and Hicher, P. Y., 2013. A simple critical state based double-yield-surface model for clay behavior under complex loading. *Acta Geotechnica*, 8(5), pp. 509-523.

Yin, Z. Y., Zhao, J. and Hicher, P. Y., 2014. A micromechanics-based model for sand-silt mixtures. *International Journal of Solids and Structures*, 51(6), pp. 1350–1363.

Yin, Z. Y., Huang, H. W and Hicher, P. Y., 2016. Elastoplastic modeling of sand-silt mixtures. *Soils and Foundations*, 56(3), pp. 520-532.

Yin, Z. Y., Hicher, P. Y., Dano, C. and Jin, Y. F., 2017. Modeling the mechanical behavior of very coarse granular materials. *Journal of Engineering Mechanics ASCE*, 143(1), pp. C401600.

An analytical theory for the capillary bridge force between spheres

N.P. Kruyt* & O. Millet**

** Department of Mechanical Engineering, University of Twente,*
P.O. Box 217, 7500 AE Enschede, The Netherlands
n.p.kruyt@utwente.nl
*** LaSIE-UMR CNRS 7356*
La Rochelle University, France
olivier.millet@univ-lr.fr

This contribution is based on Kruyt & Millet (2017).

An analytical theory has been developed for properties of a steady, axisymmetric liquid-gas capillary bridge that is present between two identical, perfectly wettable, rigid spheres. In this theory the meridional profile of the capillary bridge surface is represented by a part of an ellipse. Parameters in this geometrical description are determined from the boundary conditions at the three-phase contact circle at the sphere and at the neck (i.e. in the middle between the two spheres) and by the condition that the mean curvature be equal at the three-phase contact circle and at the neck. Thus, the current theory takes into account properties of the governing Young-Laplace equation, contrary to the often-used toroidal approximation. Expressions have been developed analytically that give the geometrical parameters of the elliptical meridional profile as a function of the capillary bridge volume and the separation between the spheres. A rupture criterion has been obtained analytically that provides the maximum separation between the spheres as a function of the capillary bridge volume. This rupture criterion agrees well with a rupture criterion from literature that is based on many numerical solutions of the Young-Laplace equation. An expression has been formulated analytically for the capillary force as a function of the capillary bridge volume and the separation between the spheres. The theoretical predictions for the capillary force agree well with the capillary forces obtained from the numerical solutions of the Young-Laplace equation and with those according to a comprehensive fit from literature (that is based on many numerical solutions of the Young-Laplace equation), especially for smaller capillary bridge volumes.

Reference

Kruyt, N.P. & Millet, O. (2017) An analytical theory for the capillary bridge force between spheres, *Journal of Fluid Mechanics* **812**, 129–151.

Solutions of Young-Laplace Equation and Stability Analysis

O. Millet*, G. Gagneux*, H. N.-G. Nguyen*, M-S. El Youssoufi, B. Mielniczuk****

** LaSIE-UMR CNRS 7356, La Rochelle University, France*
olivier.millet@univ-lr.fr
*** LMGC-UMR CNRS 5508, University of Montpellier, France*

We revisit from an inverse problem method the exact resolution of Young-Laplace equation for capillary doublets. The missing information on the pressure deficiency Δp (which is often an unknown of the problem) will be restored without the experimental device of suction control. Only the use of a digital camera with macrozoom allows to measure the suction $s = -\Delta p$ according to the observed value of the gorge radius, then compared to critical bounds. The sought value s results immediately via a set of available explicit formulas.

We establish a simple criterion based on the observation of the contact points, of the wetting angles and the gorge radius, to classify in an exhaustive way the nature of the surface of revolution: portion of nodoid, of unduloid, both with concave or convex meridian, of catenoid, of cylinder or of circular profiles (toroid). In every case, we propose an exact parametric representation of the meridian based on the observed geometry of the boundary conditions and on a first integral of Young-Laplace equation that translates a conservation energy principle.

Moreover, we prove that the inter-particle force may be evaluated on any section of the capillary bridge and constitutes a kind of specific invariant for surfaces of revolution. The proposed method leads to very convenient analytical expressions easy to use. The parameterization chosen enables a direct link between the half-axis of the conics and the observed data on the boundary. This approach spares having recourse to the simple toroidal approximation or to spline functions that do not respect (except in an exceptional theoretical case) the Young-Laplace equation.

The pertinence of the addressed approach has already been highlighted in several experimental results obtained on various geometries of capillary bridges, and has, very recently, been extended to polydisperse configurations. Moreover, the stability of solutions of Young-Laplace equations is analyzed, based on the second variation criterion of the associated potential (minimization problem under constraints), revisited through Vogel's stability criteria. A high-speed camera has been added to the experimental device to capture the rupture of capillary bridges. It complements the theoretical analysis performed. A theoretical stability criterion and conjectures on breakage will be proposed and discussed.

References

Gagneux, G., Millet, O. (2014). Analytic calculation of capillary bridge properties deduced as an inverse problem from experimental data. *Transport in porous media*, *105*(1), 117-139.

Gagneux, G., Millet, O., Mielniczuk, B., El Youssoufi, M. S. (2017). Theoretical and experimental study of pendular regime in unsaturated granular media. *European Journal of Environmental and Civil Engineering*, *21*(7-8), 840-853.

Nguyen, N.G.H., Millet, O., Gagneux, G. (2017). Exact calculation of axisymmetric capillary bridge properties between two unequal-sized spherical particles, *submitted to Mathematics and Mechanics of the solids.*

Mitigating debris flow impacts by flexible barriers: a unified predictive framework based on coupled CFD-DEM approach

Jidong Zhao & Xingyue Li

Department of Civil and Environmental Engineering, the Hong Kong University of Science and Technology, Clearwater Bay, Kowloon, Hong Kong SAR, P.R. China
Email address: jzhao@ust.hk

This study presents a unified method to simulate mitigating debris flow impacts by flexible barriers based on a coupled CFD-DEM approach. In particular, the debris flow is modelled as a mixture of a viscous fluid and a particle system by the coupled CFD-DEM approach which has been properly validated (Zhao & Shan 2013a, b; Shan & Zhao 2014). The flexible barrier is simulated as a bonded particle network with remote interactions by the DEM, a method inspired by DEM simulation of rockfall protection fence (Nicot et al. 2001; Bertrand et al. 2008; Thoeni et al. 2014). The complicated three-way interactions among the fluid in the debris mixture, the solid in the debris mixture and the barrier structure can be seamlessly considered in the coupled CFD-DEM approach.

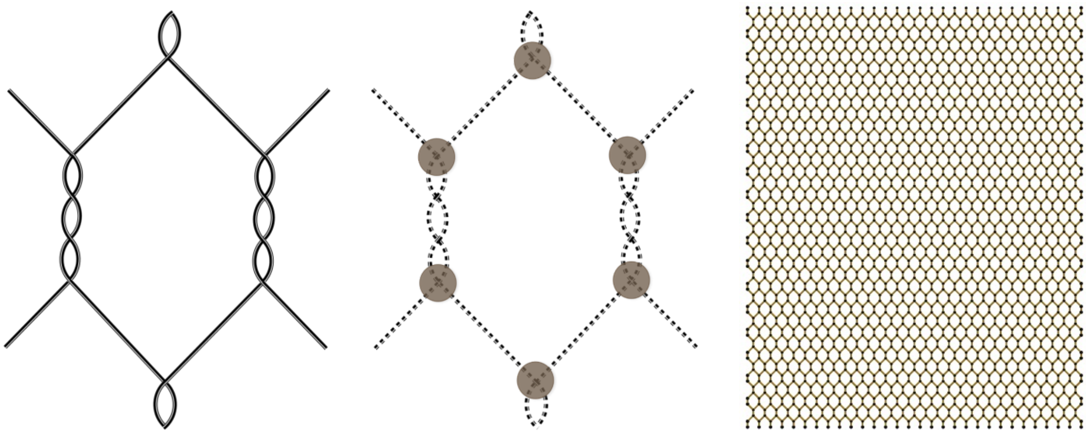

Figure 1. (a) Illustration of simulating a double-twisted wire net; (b) Discrete particles with remote interactions; (c) Discrete network for a flexible barrier formed by (b) in the DEM

While detailed formulations on a general coupled CFD-DEM approach have been explained in Zhao & Shan (2013a, b) and Shan & Zhao (2014), emphasis is placed herein upon how a flexible barrier can be conveniently simulated within the same framework of DEM. Figure 1 illustrates a hexagonal wire mesh modelled by the DEM. A real wire net is firstly discretized by a set of spherical particles placed at the physical nodes of the mesh and these nodal particles are then connected by remote interactions described by cylindrical parallel bonds which can sustain both forces and moments (Potyondy & Cundall 2004). According to beam theory in structure mechanics, the maximum tensile and shear stresses acting on the parallel-bond periphery are calculated as follows:

$$\sigma^{max} = \frac{-F^n}{A} + \frac{|M^s|}{I}R \tag{1}$$

$$\tau^{max} = \frac{|F^s|}{A} + \frac{|M^n|}{J}R \tag{2}$$

where F^n, F^s and M^n, M^s denote the axial and shear-directed forces and moments, respectively; R, A, I and J are the radius, area, moment of inertia and polar moment of inertia of the parallel-bond cross section, respectively. If the maximum tensile stress exceeds the tensile strength ($\sigma^{max} \geq \sigma_c$) or the maximum shear stress exceeds the shear strength ($\tau^{max} \geq \tau_c$), the parallel bond breaks which indicates the breakage of the corresponding wire. The nodal particles carry all the physical mass of the entire wire network and interact with the solid particles in the debris system according to the same manner (e.g., collision, contact and friction) as in conventional DEM.

As demonstrated in Figure 2, the model setup consists of an inclined channel with slope angle of θ, with a cubic debris mixture placed initially at the top of the channel and a flexible barrier at the downstream of the channel. The debris mixture of water and soil particles is initially constrained before it is released to flow down and impacts on the flexible barrier. The bottom edge and two lateral edges of the flexible barrier are fixed to mimic the anchored boundary conditions.

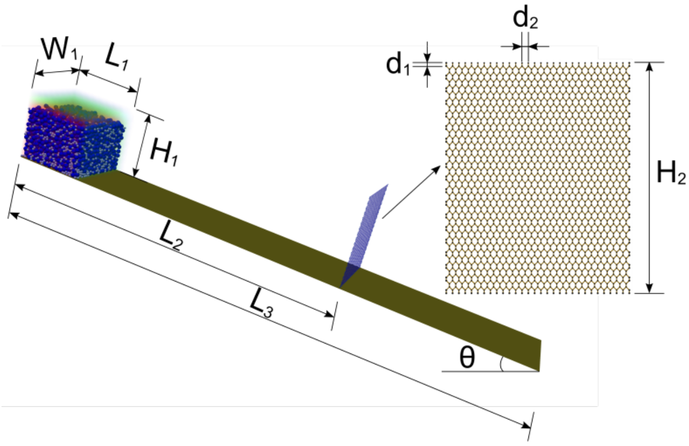

Figure 2. Model setup for a coupled CFD-DEM simulation of debris flow with a flexible barrier

This study first verifies the feasibility of the proposed CFD-DEM method in modelling debris flow mitigated by flexible barriers. Failure modes of the barrier and roles of different components in the barrier are then investigated. Both a uniform barrier net and a barrier net with reinforcing cables are considered and compared against experimental observations, theoretical predictions and other numerical simulations, to identify instructive correlations between the impact force and the controlling factors such as the slope inclination and the solid fraction in the debris mixture with consideration of the uniform barrier. In particular, our simulation results indicate that a small slope angle generally results in a low peak impact force and a small stationary impact force due to the low potential energy and the elongated deposition along the slope, respectively. The impact force can be greatly enhanced by an increasing solid fraction in the debris mixture. However, a threshold is identified beyond which further increase in solid fraction will no longer enhance the impact force, due to the dragged mobility of the debris mixture by relatively high solid fraction. In addition to uniform barriers, a barrier with reinforcing cables has also been examined under various loading conditions to investigate the deformed barrier shape, which shows good quantitative agreements with the experimental results by Ferrero et al. (2015).

Barrier failure has been a key concern for design and different failure modes may occur when a barrier is subjected to various impact conditions. As summarized in Table 1, we have observed four failure modes for a flexible barrier using various stiffnesses and strengths. Mode I is characterized by a two-step failure, the initial breakage at the bottom edge of the barrier followed by the breakage of two lateral edges. Accordingly, two local peaks are identified in the evolution of total tensile force sustained by the barrier, which occur at the instances that the bottom edge and lateral edges start to break, respectively. The barrier in Failure mode II breaks from the lower center part to around which renders a hole as demonstrated in Table 2. The accompanying evolution of total tensile force illustrates only one sharp peak at which the barrier starts to break. Failure mode III features a simultaneous breakage at the bottom edge and the center part of the barrier, which appears to be a mixed pattern of Mode I and Mode II. Nevertheless, Mode III is rarely observed in our simulations. In contrast to the mentioned three failure modes resulted from the barrier breakage, a fourth mode (Mode IV) is found with excessive deformation of the barrier mesh. The highly magnified mesh opening can lead to the passing of coarse particles in the debris mixture through the mesh, which notably reduces the capacity of the barrier and causes a small force sustained in the barrier after the dynamic impact.

Table 3. Summary of observed failure modes of flexible debris flow barrier

Failure mode	I	II	III	IV
Front view of the failed barrier	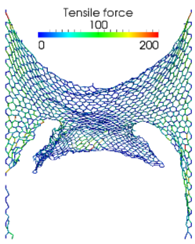	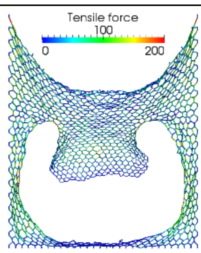	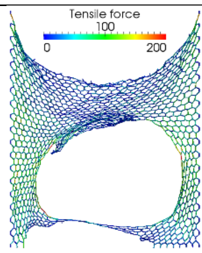	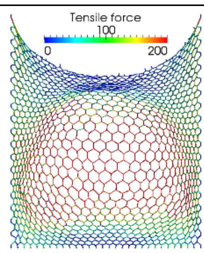
Total tensile force	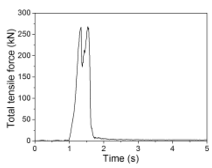	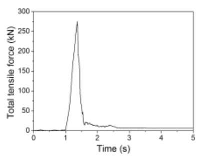	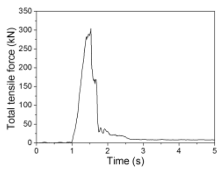	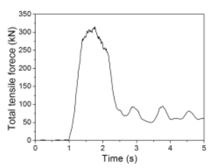
Notes	Break from bottom edge to lateral edges	Break from centre	Break from centre and bottom edge simultaneously	Excessive deformation without breakage

Whilst uniform barrier has been adopted for investigations in small-scale experiments (Wendeler & Volkwein 2015) and numerical simulations (Leonardi et al. 2016), practical applications of flexible barriers usually exploit non-uniform barriers with support cables. We investigated two non-uniform barriers, including a barrier consisting of single wires and double twists and a barrier composed by single wires, double twists and cables, to explore the role of different components in a non-uniform barrier. A uniform barrier was examined as a basis for comparison. Our simulation results clearly demonstrate that both the impact force and the deformation of the barrier are greatly reduced with the strengthening effect of the double twists and cables. Meanwhile, the retained debris mass was increased with the incorporation of double twists and cables in a barrier, due to the small deformation and the less magnified mesh opening. In contrast to the marginal effect of double twists on the force distribution within the barrier, the cables may bear a significant proportion of the total impact force once used in a barrier, which reflects its effectiveness in transferring the loads from the barrier net. Practical design of flexible barriers should therefore include cables as an essential reinforcing component.

Acknowledgements

The research reported in this study was financially supported by the University Grants Council of Hong Kong by a Theme-based Research Scheme project T22-603/15N.

References

Bertrand, D., Nicot, F., Gotteland, P. and Lambert, S., 2008. Discrete element method (DEM) numerical modeling of double-twisted hexagonal mesh. *Canadian Geotechnical Journal*, *45*(8), pp. 1104-1117.

Ferrero, A. M., Segalini, A. and Umili, G., 2015. Experimental tests for the application of an analytical model for flexible debris flow barrier design. *Engineering Geology*, *185*, pp. 33-42.

Leonardi, A., Wittel, F. K., Mendoza, M., Vetter, R. and Herrmann, H. J., 2016. Particle–Fluid–Structure Interaction for Debris Flow Impact on Flexible Barriers. *Computer-Aided Civil and Infrastructure Engineering*, *31*(5), pp. 323-333.

Nicot, F., Cambou, B. and Mazzoleni, G., 2001. Design of rockfall restraining nets from a discrete element modelling. *Rock Mechanics and Rock Engineering*, *34*(2), pp. 99-118.

Potyondy, D. O. and Cundall, P. A., 2004. A bonded-particle model for rock. *International Journal of Rock Mechanics and Mining Sciences*, *41*(8), pp. 1329-1364.

Shan, T. and Zhao, J., 2014. A coupled CFD-DEM analysis of granular flow impacting on a water reservoir. *Acta Mechanica*, *225*(8), pp. 2449.

Thoeni, K., Giacomini, A., Lambert, C., Sloan, S. W. and Carter, J. P., 2014. A 3D discrete element modelling approach for rockfall analysis with drapery systems. *International Journal of Rock Mechanics and Mining Sciences*, *68*, pp. 107-119.

Wendeler, C. and Volkwein, A., 2015. Laboratory tests for the optimization of mesh size for flexible debris-flow barriers. *Natural Hazards & Earth System Sciences*, *15*(12).

Zhao, J. and Shan, T., 2013a. Numerical modeling of fluid-particle interaction in granular media. *Theoretical and Applied Mechanics Letters*, *3*(2).

Zhao, J. and Shan, T., 2013b. Coupled CFD–DEM simulation of fluid–particle interaction in geomechanics. *Powder Technology*, *239*, pp. 248-258.

A 1D higher order gradient mixture model for rocks for the high frequency regime

L. Placidi*, E. Barchiesi **, and J. Fortin***

**Engineering Faculty, International Telematic University Uninettuno. Corso Vittorio Emanuele II, 39 00186 Roma, Italy*
*** Università degli Studi di Roma La Sapienza, Department of Structural and Geotechnical Engineering, Roma, Italy*
**** Laboratoire de Geologie de l'Ecole Normale Superieure, PSL-University, Paris, France*
Email address: luca.placidi@uninettunouniversity.net

Introduction

It has been known since the first half of the 19th century, namely since the pioneering works by Gabrio Piola, (e.g. dell'Isola et al., 2015), that many micro-structural effects in mechanical systems can be modeled by means of continuum theories.
This can be found in the literature for both monophasic systems, bi-phasic or granular materials.
Unlike classical Cauchy continua, second and higher order continua are better used for investigating microstructural effects as well as for detecting high frequency (low wave-length) wave propagation.
The aim of this work is to provide a model that can predict a dispersion relation in the high frequency regime. The purpose of this model is to provide a better interpretation of interesting experimental results in Fortin et al, (2014) obtained by the third author, which consist of measuring elastic wave velocity in the same frequency regime.
Thus, we aim to define a model for rocks that is as simple as possible and, at the same time, useful for interpreting standard results of phase velocities and the attenuation coefficients that are generally measured in the labs and in the field. Thus, we will not consider the most possible general theory but only a theory that possess a minimum number of constitutive coefficients for this purpose.
For this purpose, we have developed a mixture model as in Placidi *et al*. (2008); on one hand, we adopt the 1D simplification and on the other hand, we consider the higher order effect as in dell'Isola *et al.* (2009).

Kinematics of the 1D problem

The 1D body that is considered in this extended abstract is a solid fluid mixture. In other words, we have two reference configurations, one for the solid (where the particles are named by the coordinate $X_s \in [0, L]$) and one for the fluid (where the particles are named by the coordinate $X_f \in [0, L]$)). Any position in the actual configuration

$$x = \chi_s(X_s, t)) = \chi_f\left(X_f, t\right)$$

is given by the superposition of two placements, $\chi_s(X_s, t))$ and $\chi_f(X_f, t))$, so that we can define two displacement fields,

$$u_s(X_s, t) = \chi_s(X_s, t) - X_s,$$

and

$$u_f(X_f, t) = \chi_f(X_f, t) - X_f,$$

one for the solid, the displacement u_s , and one for the fluid, the displacement u_f. Besides another placement is defined function $\phi(X_s, t)$, as well as another displacement function $\varphi(X_s, t)$ on the solid domain $X_s \in [0, L]$ that gives, for any solid particle X_s, the fluid particle X_f that occupies the same position x of the solid particle X_s, i.e.,

$$X_f = \phi(X_s, t) = X_s + \varphi_s(X_s, t).$$

A graphical representation of the kinematic of the mixture that is here used and of the interpretation of the placements functions $\chi_s(X_s, t))$, $\chi_f(X_f, t))$ and $\phi(X_s, t)$ is shown in Fig. 1.

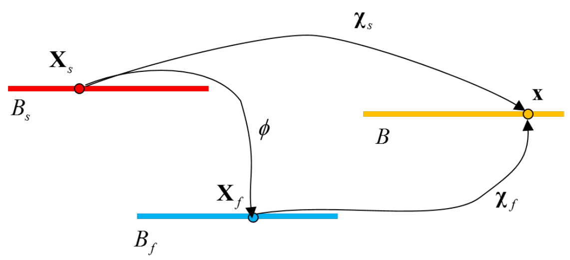

Figure 1. Kinematics of the 1D mixture.

Plane wave solution

We adopt an extended Rayleigh-Hamilton principle with a proper definition of the action functional in terms of kinetic, strain and external energy functionals. Such functionals take into account not only the standard terms of each phase of the mixture but also their interactions and second gradient terms. In particular, the kinetic energy functional contains micro-inertia terms, the strain energy functional second gradient terms and the external energy functional the possibility to have not only force but also double force.

Finally, the system of Partial Differential Equations are found and solved in terms of plane waves with a given frequency ω and wave number k. Keeping this in mind, phase velocity V_{ph},

$$V_{ph} = Re\left(\frac{\omega}{k}\right),$$

and attenuation coefficient A

$$A = -2\frac{Im(k)}{Re(\omega)}$$

have been calculated. They are shown in Fig. 2. On the basis of these results we observe, in the phase velocity graphic, the presence of three regimes, that are really observed in the experiments. In correspondence of each transition, i.e. at the same frequency at which the transition occurs, we observe, in the attenuation graphic, a peak. It is possible show from a numerical point of view that the first transition (at lower frequencies) is obtained because of the presence of the conceived two dynamics, one of the solid and one of the fluid, of the mixture. Besides, the second transition (at higher frequencies) is obtained because of the inclusion of a higher order term.
It is finally worth noting that the same qualitative behaviour has also been observed in the experiments.

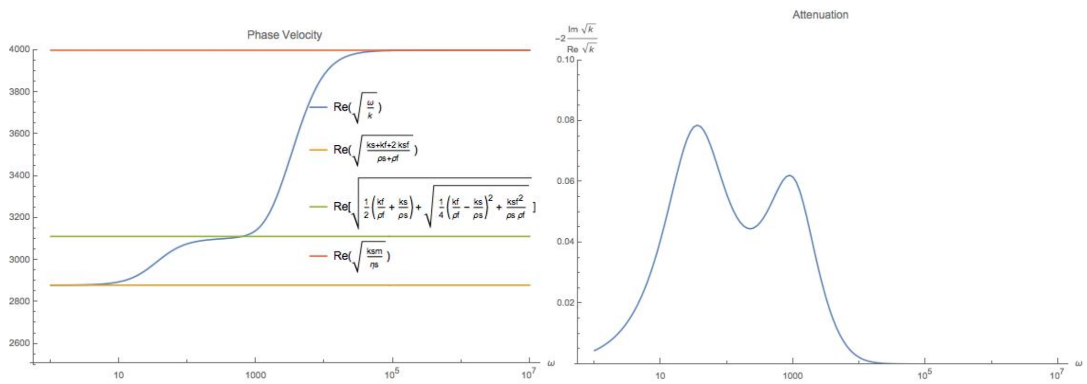

Figure 2. On the left hand side, we have the numerical solution of plane wave velocity and on the right hand side that of the attenuation coefficient.

Conclusions

A 1D model for saturated solid-fluid mixtures is derived with the inclusion of higher order terms and through a variational procedure. The model is conceived to obtain a well-posed system of Partial Differential Equations that can take into account the transitions from drained, undrained and unrelaxed regimes. The first transition (at lower frequencies) is obtained because of the conceived two dynamics of the mixture. The second transition (at higher frequencies) is obtained because of the inclusion of a higher order term.

References

dell'Isola Francesco, Andreaus Ugo, Placidi L (2015). At the origins and in the vanguard of peridynamics, non-local and higher gradient continuum mechanics. An underestimated and still topical contribution of Gabrio Piola. *Mathematics and Mechanics of Solids*, vol. 20, p. 887-928, ISSN: 1081-2865, doi: 10.1177/1081286513509811

J Fortin, L Pimienta, Y Guéguen, A Schubnel, E.C David, M Adelinet, Experimental results on the combined eects of frequency and pressure on the dispersion of elastic waves in porous rocks, The Leading Edge 33 (6), 648-654, 2014

Placidi L, dell'Isola Francesco, Ianiro Nicoletta, Sciarra Giulio (2008). Variational formulation of pre-stressed solid-fluid mixture theory, with an application to wave phenomena. EUROPEAN JOURNAL OF MECHANICS. A, SOLIDS, vol. 27(4), p. 582-606, ISSN: 0997-7538, doi: 10.1016/j.euromechsol.2007.10.003

dell'Isola, F., Madeo, A., & Seppecher, P. (2009). Boundary conditions at fluid-permeable interfaces in porous media: A variational approach. International Journal of Solids and Structures, 46(17), 3150-3164.